Climate Dynamics (2023) 61:5551–5572
https://doi.org/10.1007/s00382-023-06870-z

Spatiotemporal variations of precipitation during the rainy season over the three-rivers headwater region of tibetan plateau from 1990 to 2020

Jingshu Zhu[1,3] · **Huizhi Liu**[2] · **Yaohui Li**[4] · **Lujun Xu**[1,3] · **Qun Du**[1,3] · **Xianhong Meng**[3,5] · **Yang Liu**[1,3]

Received: 8 April 2023 / Accepted: 18 June 2023 / Published online: 27 June 2023

Abstract

The Three-River Headwater Region (TRHR) has undergone significant hydrological changes and affects the water resources security in the local and downstream areas. We use multiple observational precipitation product, as well as the ERA5 reanalysis dataset to investigate the precipitation variations over the TRHR during the rainy season from 1990 to 2020, and to analyze the contributions of local evaporation and remote water vapor transport to the precipitation and its variations. The precipitation shows a significant increasing trend (17.8 mm decade^{-1}). The precipitation variability (PV) is larger at daily scale and smaller at interannual scale. The spatial distribution of PV varies on different timescales, which reflects the different dominant regimes driving the moisture transport. The mean precipitation in the TRHR is predominantly contributed by western and southern moisture influxes, and the increasing trend of these influxes (10.8 kg s^{-1} decade^{-1}) determines the precipitation increase. Local evaporation provide about 6% of water vapor for the precipitation, while it has little influence on the precipitation change. The anomalous precipitation in wet and dry years is mainly controlled by the atmospheric circulation over the Tibetan Plateau, which regulates the southwestern moisture transport towards the TRHR. Additionally, the precipitation during 1990–2020 increases by about 3.9% compared to that during 1960–1989. It is related to the higher conversion ratio of water vapor influxes to precipitation and larger evaporation over the TRHR. These findings improve our understanding of the precipitation variations in the TRHR and provide insights for policy makers to optimize water resources management to cope with the global climate change.

Keywords Precipitation variation · Water vapor transport · Long term · Rainy season · TRHR

1 Introduction

The Tibetan Plateau (TP), known as the third pole of the world (Qiu et al. 2008), is the headwater of many Asian great rivers (i.e. the Yangzi, Yellow, Lantsong, Salween, Mekong, Ganges, Indus, and Yarlung Zangbo rivers) (Cuo et al. 2019). The TP is a very sensitive area to climate change. Over the past several decades, it has undergone a rapidly warming and wetting change, and the warming rate is more than twice as high as other regions (Rangwala and Miller 2012). Although the precipitation over the TP shows large spatiotemporal variability, the increasing trend of precipitation is supported by the various ground observational precipitation datasets (Gao et al. 2014; You et al. 2008; Yao et al. 2012). It has a profound impact on the survival and development of more than one billion people in the downstream areas (Qiu 2008; Radic et al. 2008).

✉ Huizhi Liu
huizhil@mail.iap.ac.cn

[1] Institute of Atmospheric Physics, Chinese Academy of Sciences, Beijing, China

[2] Department of Atmospheric Sciences, Yunnan University, Kunming, China

[3] College of Earth and Planetary Sciences, University of Chinese Academy of Sciences, Beijing, China

[4] College of Aviation Meteorology, Civil Aviation Flight University of China, Guanghan, China

[5] Northwest Institute of Eco-Environment and Resources, Chinese Academy of Sciences, Lanzhou, China

The Three-River Headwater Region (TRHR) , located in the hinterland of the Tibetan Plateau, is known as the “Water Tower” of Asia. It is a significant water source region for the Yangtze River, the Yellow River and the Lantsang River (Cao and Pan 2014; Fan and Wang 2011; Shao et al. 2017; Zhang et al. 2012). The mean annual runoff in the TRHR is about 425.8×10^8 m^3 (Wang et al. 2007; Shao et al. 2017; Zhang et al. 2012), which supplies to approximately 25%, 49% and 15% of the total water volume of the Yangzi, Yellow and Lantsang rivers, respectively (Meng et al. 2020). The TRHR is a high-altitude mountainous area with the mean altitude over 4000 m (Shang et al. 2021; Shi et al. 2016). It has the largest and highest alpine wetland ecosystem on earth (Tong et al. 2014b). The amplification of global warming over the TRHR intensifies the spatiotemporal precipitation variability, which plays a key role in lakes and wetlands expansion, runoff increase and biodiversity maintenance through the interaction of multiple hydrological factors (Tong et al. 2014b; Zhang et al. 2011).

The water vapor required for the precipitation are mainly supplied by remote water vapor transport and local evaporation (Guo et al. 2018; Zhao and Zhou 2021). Water vapor transport is one of the most active hydrological cycle factors, and has great impact on the precipitation (Wang et al. 2021). The southern water vapor transported to the TRHR originates from the Arabian Sea, the South China Sea, and the Bay of Bengal (Feng and Zhou 2012; Simmonds et al. 1999) , and is mainly affected by the South Asia monsoon. Although most of the water vapor transport from the distant oceans is deflected to Southeast China, quite a bit of water vapor climbs across the TP towards the TRHR under the integration of mechanical and thermal forcing (Xu et al. 2014). The northern water vapor transport is affected by the westerlies, and it is originated from the Central Eurasia (Ma et al. 2018; Shen et al. 2021; Zhang et al. 2019; Zhou et al. 2019a). The water vapor transport is influenced by large-scale atmospheric circulations, such as the sea surface temperature anomalies in the Pacific, Indian, and North Atlantic oceans, as well as the Atlantic multi-decadal oscillation (Bothe et al. 2010; Li et al. 2014; Ren et al. 2017).

The extent of the evaporation effect on the precipitation reflects the region moisture and the intensity of land–atmosphere interaction (Koster et al. 2004; Seneviratne et al. 2010). In wet conditions, the evaporation is mainly determined by the radiation budget, and it is negatively correlated with precipitation. In dry conditions, the evaporation is regulated by the soil moisture, more evaporation can promote the precipitation, although the effect is usually too small (Guo et al. 2018). In Southeast China, the local evaporation has little impact on the precipitation. While in the TP, the complex terrain confines the evaporation, thus it has strong effect on the precipitation (van der Ent et al. 2010). The TRHR is a semi-humid and semi-arid region, and the effects of evaporation on precipitation varies at the seasonal timescales. In addition, the effect is sensitive to the boundary stability (Guillod et al. 2014; Seneviratne et al. 2010; Taylor et al. 2012). Due to the higher altitude of the TRHR than the lowland regions, more solar radiation incomes to the surface, thus more water vapor from the boundary layer is heated and lifted to the upper level, which promotes the convective events (Sugimoto and Ueno 2010).

Numerous studies have found that the precipitation in the TRHR has significant annual and seasonal variations by using observational datasets (Sang, et al. 2013; Sun and Wang 2014; Yang et al. 2014; Zhang et al. 2019). The annual precipitation in the TRHR increases weakly from 1960 onward, with an abrupt change around 2002 (Liu et al. 2019). At the seasonal scale, the precipitation in the TRHR increases in winter and spring and decreases in summer and autumn during 1960–2010 (Yi et al. 2013). The precipitation variations in the TRHR shows greatly spatial heterogeneity. It reduces in the northern and western TRHR, and increases in the eastern and southern TRHR (Meng et al. 2022). The extreme temperature and precipitation indices have significant variations in the TRHR (Cao and Pan 2014; Ding et al. 2018). The indices of very wet day precipitation, extremely wet day precipitation, simple daily intensity, wet day precipitation, heavy precipitation days exhibit increasing trends over the TRHR (Cao and Pan 2014; Liang et al. 2013; Shi et al. 2016). The number of consecutive dry days displays a downward trend (Xi et al. 2018; Zhao et al. 2021). These significant variations occur over the northern TRHR. The rainy season (June–September) precipitation, accounting for 76% of the annual precipitation (Li et al. 2009). The rainy season precipitation exerts strong effects on the surface energy balance, the soil water content, and the plants productivity in the TRHR (Yang et al. 2022). Natural disasters, such as avalanches, mudslides, and floods induced by heavy precipitation could restrict the economic developments in the TRHR. It is necessary to shed light on the rainy season precipitation in the area. The water vapor transport associated to the rainy season precipitation over the TP has been discussed in several studies (Feng and Zhou 2012; Gao et al. 2014; Sun and Wang 2018, 2019; Wang et al. 2017). The primary water vapor source of the precipitation over the TP comes from the Indian subcontinent to the southern hemisphere, the Bay of Bengal and the northwestern TP (Chen et al. 2012). The mid-latitude westerly has a high share in the water vapor transport over the TP. The Southwest monsoon is limited by the mountain regions in the TP (Curio et al. 2015). The northern TP is mainly affected by the westerlies, and the southern TP is regulated by the monsoons (Yao et al. 2012; Ma et al. 2018; Song et al. 2022; Zhou et al. 2019a, b). The water vapor content and moisture budget show an increasing trend over the TP during recent years (Yu et al. 2020). The warming northwestern Atlantic make important contribution to the wetting trend at the inter-decadal scale (Zhou et al. 2019b). At the interannual scale, the precipitation increase is contributed by the enhanced water vapor source from the neighboring eastern regions (Zhao et al. 2021). The impact of evaporation on the precipitation remains an uncertain issue (Curio et al. 2015; Joswiak et al. 2013). The deep convections driven by surface heat flux over the TP are generally weaker and less organized due to lower water vapor content and CAPE, thus the precipitation is largely sensitive to local evaporation in the TP (Sugimoto and Ueno 2010; Wei et al. 2019; Zhu and Chen 2003). The precipitation recycling ratio (Pr) is an important indicator to measure the contribution of local evaporation and horizontal water vapor transport (Zhao and Zhou 2021). The local evaporation is fully mixed with external water vapor transport first, then part of the water vapor export from the target region, and the residual forms to the precipitation (Guo et al. 2018; Zhao et al. 2021). It is worth noting that the Pr is regulated by the shape and area of the target region (Harding and Snyder 2012). The Pr has a linear relationship in logarithm coordinates with the regions, and it increases with the area (Bisselink and Dolman 2008; Dominguez et al. 2006; Hua et al. 2017). The Pr over the TP vary from less than 10% to more than 60% by using different methods (An et al. 2017; Curio et al. 2015; Sun and Wang 2014; Zhang et al. 2017; Zhang et al. 2019).

Due to the difference of the examined timescales and regions, there are no unified conclusions on the precipitation variations in the TRHR. The previous studies have not explicitly analyzed the relative importance of the two factors on the precipitation. In this study, we use the ERA5 dataset to investigate the long-term variations of the rainy season precipitation in the TRHR from 1990 to 2020, and its associated potential atmospheric mechanisms. Rest of this paper is arranged in the following. In Sect. 2, we introduce the data and methods used. Section 3 presents the interannual changes of the rainy season precipitation in the TRHR, and the contributions of water vapor transport and the local evaporation to the precipitation. Section 4 discusses the possible mechanisms for the precipitation variations in the TRHR. The major conclusions are shown in Sect. 5.

2 Data and method

2.1 Data

(1) Rain gauge observations

The TRHR is located in the southern part of Qinghai Province (31° 39′–36° 16′ N, 89° 24′–102° 23′ E), with a basin area of 3×10^5 km^2 (Meng et al. 2020). There are 12 meteorological stations with the complete daily precipitation during 1990–2020 in the TRHR (Fig. 1; Table 1). The data are obtained from the China Meteorological Administration Center (CMA). To ensure data quality, these observations are screened by quality control. The outliers and data that do not include at least 20 valid values per month are discarded. After filtering, there are seven stations with 31 years con-

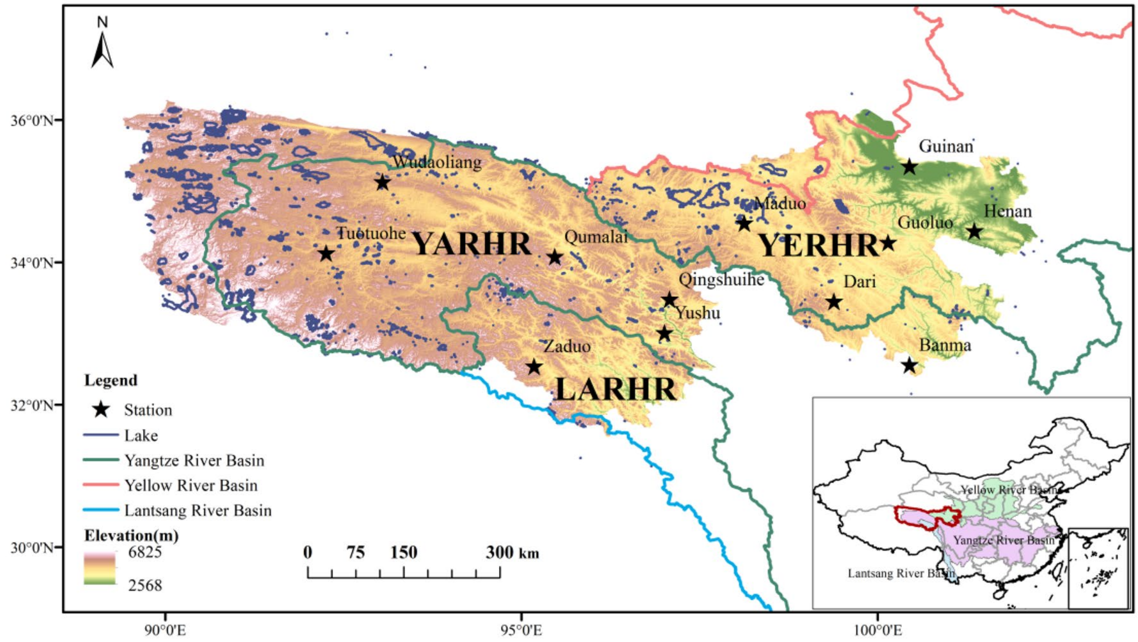

Fig. 1 Terrain height of the TRHR, units: m. The stars denote the locations of meteorological stations, and the lines denote lakes and the three rivers originated from TRHR

Table 1 Meteorological Stations on the TRHR

	Station	Elevation m	Longitude °E	Latitude °N	Period of record
YARHR	Wudaoliang	4614.2	93.05	35.13	1979–2020
	Tuotuohe	4534.3	92.26	34.13	1992–1998, 2000–2020
	Qumalai	4176.4	95.47	34.08	1979–2020
	Qingshuihe	4417.5	97.08	33.48	1979–2020
	Yushu	3682.2	97.01	33.01	1979–2020
	Banma	3530	100.45	32.56	1979–2020
YERHR	Dari	3968.5	99.39	33.45	1992–1998, 2000–2020
	Guinan	3201.6	100.45	35.35	2001–2020
	Maduo	4273.3	98.13	34.55	1992–1998, 2000–2020
	Guoluo	3720	100.15	34.28	1979–2020
	Henan	3501	101.36	34.44	1979–2020
LARHR	Zaduo	4068.5	95.18	32.54	1992–1998, 2000–2020

tinuous data, four stations with 1 year data gap, and one station with 76 useful months data. We use the Heidke skill score (HSS; Wilks 1995) to estimate the accuracy of ERA5 for daily precipitation forecasts. To compare the ERA5 precipitation with the rain gauge observation, the gridded precipitation data in the ERA5 is taken with bilinear interpolation.

(2) ERA5

ERA5 is the fifth generation of atmospheric reanalysis data from the European Centre for Medium-Range Weather Forecasting (ECMWF). It has combined the advanced climate model and assimilation system with observations to form a complete global reanalysis datasets since 1979, including the atmosphere, land, and ocean variables (Hersbach et al. 2020). ERA5 has a higher spatiotemporal resolution (0.25°×0.25°, 37 level, 1 h) and more rich variables compared with other reanalysis data. In this study, the daily and monthly precipitation, air temperature, pressure, evapotranspiration, cloud cover, wind, vertical velocity, and specific humidity from the surface to 300 hPa are selected for examination (Xu et al. 2008).

(3) CMFD

Owing to the sparse and uneven distribution of meteorological stations in the TRHR, the regional climatic precipitation features are usually not represented by station data. We also compare the ERA5 precipitation with the China Meteorological Forcing Data datasets (CMFD) data. The CMFD is a near-surface meteorological reanalysis dataset developed by the Institute of Tibetan Plateau Research at the Chinese Academy of Sciences (He et al. 2020; Yang et al. 2010). The dataset provides the 2 m-temperature (K) , 2 m-specific humidity (kg kg^{-1}) , 2 m-air pressure (Pa) , 10 m-wind speed, downward long-wave radiation (W m^{-2}) ,downward short-wave radiation (W m^{-2}) at the surface and precipitation rate (mm 3 h^{-1}) , with a spatial resolution of 0.1° and a temporal resolution of 3-h. The CMFD is produced by combining the China Meteorological Administration (CMA) station data, TRMM precipitation (3B42) , GEWEX-SRB downward shortwave radiation, GLDAS data and Princeton forcing data. The CMFD has low bias and strong correlations with observation, thus it has great advantages in analyzing the precipitation over the TP (Wu et al. 2019). In this study, the Pearson correlation coefficient (r) , mean deviation (MD) , and mean absolute deviation (MAD) were used for the assessment.

(4) TRMM Precipitation

The Tropical Rainfall Measuring Mission (TRMM) is a joint space mission combining the National Aeronautics with Space Administration (NASA) and the Japanese Aerospace Exploration Agency (JAXA) to estimate the precipitation over the tropical regions (Shrivastava et al. 2014). TRMM is equipped with five kinds of remote sensing instruments: Visible and Infrared Scanner (VIRS) , TRMM Microwave Imager (TMI) , Precipitation Radar (PR) , Lightning Imaging Sensor (LIS) and the Cloud and the Earth's Radiant Energy System (CERES). The VIRS, TMI and PR are the basic precipitation measurement instruments (Kummerow et al. 1998). TRMM was launched at Nov27,1997, and stopped receiving the data until Apr16,2015. The subsequent data is provided by the GPM (Global Precipitation Measurement).

TRMM has been previously used to investigate the precipitation features, deep convection and precipitation vertical structure over the TP (Houze et al. 2007; Qie et al. 2014; Xu et al. 2011) , analyze the linkages between the precipitation, clouds, atmospheric circulation, and topography over northern India and Himalayas (Barros et al. 2004) , to and to evaluate and calibrate the precipitation data from reanalysis datasets and atmospheric model simulations (He et al. 2017; Tong et al. 2014a; Maussion et al. 2011, 2014). In this study, TRMM_3B42 Version 7, which has a 3-h temporal resolution and a spatial resolution of 0.25-degree to evaluate the rainy season precipitation over the TRHR (Huffman et al. 2007). It covers the regions between 50 °S and 50 °N.

2.2 Statistical analysis

(1) Precipitation variability

The precipitation variability (PV) of different typical timescales: synoptic (2–10 days) , monthly (25–35 days) , and inter-annual (1–8 years) is estimated as the standard deviation of the band-pass Lanczos filtered time series of daily precipitation, and the daily PV is the standard deviation of unfiltered time series (Pendergrass et al. 2017; Zhang et al. 2021).

(2) EEMD (Ensemble Empirical Mode Decomposition)

Empirical mode decomposition (EMD) is an empirical and adaptive method, which decomposes the time series into intrinsic mode functions (IMF) and residuals (RES) , showing the variable features at different timescales (Huang et al. 1998). EEMD is improved from the EMD to make the decomposition results more reasonable. It is generally used to describe the fluctuation of meteorological and hydrology elements (Chen et al. 2020). The procedures of the EEMD can be summarized in the following (Roushangar and Alizadeh 2018; Basha et al. 2015) :

1. Add a random white noise sequence to the targeted time series.
2. Decompose the series with the white noise into IMFs using the EMD method.
3. Repeat Step 1 and Step 2 with different white noise series each time.
4. Average the ensemble IMFs and the residuals.

2.3 Precipitation recycling ratio

As shown in Eq. 1, regional water vapor changes can be described by the mass conservation of water vapor:

$$\frac{\partial Q}{\partial t} + \frac{\partial F_u}{\partial x} + \frac{\partial F_v}{\partial y} - E + P = 0 \tag{1}$$

Q is the vertically integrated moisture fluxes (kg m^{-2}) ; F_u and F_v are the vertically integrated advected water vapor fluxes (kg m^{-1} s^{-1}) , respectively. E and P are the evaporation (including the transpiration) and the precipitation (kg m^{-2} s^{-1}) , respectively. The $F_u$andF_v over the TRHR are calculated using ERA5 reanalysis at 10 pressure layers (ground, 700, 650, 600, 550, 500, 450, 400, 350, 300 hPa, Trenberth 1991; Huang et al. 2015) :

$$\begin{cases} F_u = \frac{1}{g}\int_{p_s}^{p_t} qudp \\ F_v = \frac{1}{g}\int_{p_s}^{p_t} qvdp \end{cases} \tag{2}$$

where p, u, v, g and q denote the air pressure (hPa) , u-component wind (m s^{-1}) , v-component wind (m s^{-1}) , gravity acceleration (m s^{-2}) and specific humidity (kg kg^{-1}) , respectively.

It is described in Eq. 1 that the regional water vapor increases by the moisture convergence and evaporation, and decreases by the precipitation. The changes of total water vapor storage are much smaller than the moisture fluxes variations at monthly and longer timescales (Guo et al. 2018; Yang et al. 2022) , thus the water vapor conservation equation can be written as:

$$\frac{\partial F_u}{\partial x} + \frac{\partial F_v}{\partial y} = E - P \tag{3}$$

In this equation, the water vapor convergence is presented as the difference of precipitation and evaporation. To better understand the regional water vapor and precipitation variations in the TRHR, we use the method B1993, which is a bulk method established by Brubaker et al (1993) to estimate the precipitation recycling ratio (Pr).The method is based on three assumptions: (1) The water vapor from remote transport and local evaporation is well-mixed in the vertical direction; (2) With the precipitation formation, the external water vapor linearly decays and the evaporation linearly increases from the upwind to the downwind direction; (3) All the grids in the target region have same values of precipitation and evaporation. Based on the Gauss divergence theorem, we rewrite the Eq. (3) as:

$$F_{in} - F_{out} = E - P \tag{4}$$

The F_{in} and F_{out} are the water vapor influx and outflux to the region, respectively. The Pr has an analytical solution with Eq. (5) :

$$Pr = \frac{E \times A}{E \times A + 2F_{in}} = \frac{P_e}{P} \tag{5}$$

$$Fr = 1 - Pr = \frac{2F_{in}}{E \times A + 2F_{in}} = \frac{P_a}{P} \tag{6}$$

$$Er = \frac{P \times A}{E \times A + 2F_{in}} = \frac{P_e}{E} \tag{7}$$

where E is the regional average evaporation (kg $\mathrm{m^{-2}\ s^{-1}}$), $\mathrm{F_{in}}$ is the vertical integration of horizontal water vapor influxes (kg $\mathrm{s^{-1}}$) ; Pe is the precipitation contributed by the evaporation; Pa is the precipitation contributed by external water vapor transport; and A is the size of target region ($\mathrm{m^2}$). In this equation, Pr means the fraction of precipitation that originates from the local evaporation. Equation 6 describes the Fr as the fraction of precipitation that originates from the external water vapor transport. The evaporation recycling ratio (Er) is expressed in Eq. (7) as the proportion of evaporation that returns to the same region in the form of precipitation. The regional external moisture conversion is mainly evaluated by E/P, which is related to the climate regime of the target region (Curio et al. 2015). Under the same climate regime, the Pr is proportional to the region areas.

In this study, the TRHR is defined as a rectangular area (30–37 °N, 90–103 °E) to calculate the water vapor transport from four directions.

$$\begin{cases} F_W = \int_{\lambda_S}^{\lambda_N} F_{\lambda_W} \cdot ad\varphi \\ F_E = -\int_{\lambda_S}^{\lambda_N} F_{\lambda_E} \cdot ad\varphi \\ F_s = \int_{\lambda_W}^{\lambda_E} F_{\varphi_s} \cdot acos\varphi_s d\lambda \\ F_N = \int_{\lambda_W}^{\lambda_E} F_{\varphi_N} \cdot acos\varphi_N d\lambda \end{cases} \tag{8}$$

$$\mathrm{F_{net} = F_{S+}F_N + F_{W+}F_E} \tag{9}$$

$\mathrm{F_S}$, $\mathrm{F_N}$, $\mathrm{F_W}$, $\mathrm{F_E}$, and $\mathrm{F_{net}}$ are the water vapor transport from southern, northern, western, eastern boundaries and the net water vapor budget, respectively; λ and φ denote the longitude and latitude; a is the earth radius (6.37×10^6 m). The Fr in four directions are written as:

$$\begin{cases} Fr_w = \frac{2F_{in}^W}{E\times A+2F_{in}} \\ Fr_e = \frac{2F_{in}^E}{E\times A+2F_{in}} \\ Fr_s = \frac{2F_{in}^S}{E\times A+2F_{in}} \\ Fr_n = \frac{2F_{in}^N}{E\times A+2F_{in}} \end{cases} \tag{10}$$

$$Fr = Fr_w + Fr_e + Fr_s + Fr_n \tag{11}$$

where $F_{in}^W, F_{in}^E, 2F_{in}^S\ and\ 2F_{in}^N (kgs^{-1})$ are the moisture influxes through the western, eastern, southern and northern boundaries to the TRHR; and $Fr_w, Fr_e, Fr_s\ and\ Fr_n$ are the contributions of water vapor from the four directions to the Pa.

3 Results

3.1 Evaluation of the ERA5 precipitation product in the TRHR

(1) Daily precipitation

The comparation of regional daily average precipitation in the TRHR and all three sub-regions [the headwater region of the Yangzi River (YARHR) , the Yellow River (YERHR) , and the Lantsang River (LARHR)] between ERA5 and CMFD are shown in Fig. 2. The results indicate that ERA5 has high fidelity in reproducing the distribution of rainy season precipitation and its annual variability. The correlation coefficients between the two datasets are all above 0.65 in the TRHR and three sub-regions. ERA5 tends to overestimate the precipitation in the TRHR, especially in the YERHR and LARHR.

(2) Precipitation frequency

The HSS indicates the capability of the simulation that is better or worse than a random simulation (Maussion et al. 2014). The range of HSS is [− 1, 1] and the equation is in the following:

$$HSS = \frac{2(f_{RR}f_{NN} - f_{RN}f_{NR})}{(f_{RR+}f_{NR})(f_{NR} + f_{NN}) + (f_{RR+}f_{NR})(f_{NR} + f_{NN})} \tag{12}$$

where f_{RR}, f_{RN}, f_{NR}, and f_{NN} represent the frequency of the four cases in Table 2, respectively.

The histograms of daily average precipitation at the stations, ERA5 and TRMM are shown in top panel of Fig. 3. Both the ERA5 and TRMM underestimate the frequency of precipitation with the intensity of more than 10 mm $\mathrm{d^{-1}}$ in the TRHR, especially in the YARHR. This confirms the findings of previous studies (Heikkila et al. 2011; Maussion et al. 2011; Su et al. 2013) demonstrating that the negative effect of rough resolution on reproducing the precipitation over the regions with complex terrain. The YARHR is the largest sub-regions among the three sub-regions, with the highest altitude and the most complex topography. It is difficult to capture local extreme convective-precipitation (Gao et al. 2018). ERA5 and TRMM have a better performance in estimating the precipitation ranged in 10–20 mm $\mathrm{d^{-1}}$ in the YERHR and LARHR. The observational records indicate that the number of precipitation events with the range of 0–10 mm $\mathrm{d^{-1}}$ accounts for approximately 80% of the total precipitation events, while ERA5 overestimates the proportion to more than 95%. The HSS, which are shown in Fig. 3e–h, reflects the capacity of ERA5 and TRMM in simulating the precipitation variations. The HSS in the TRHR shows an increasing–decreasing trend with the precipitation increase, and the peak occurs at 4–5 mm $\mathrm{d^{-1}}$. ERA5

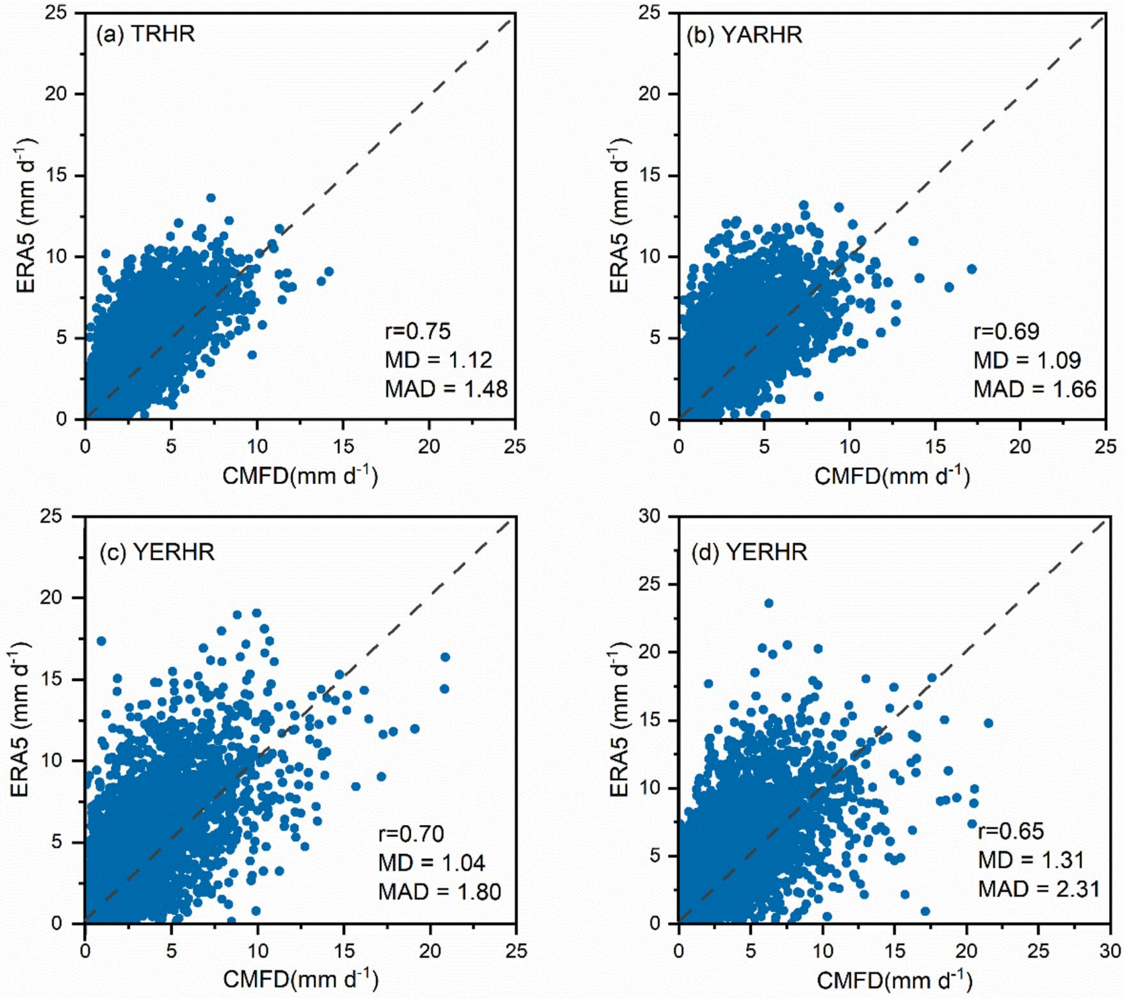

Fig. 2 Comparison of regional average of daily precipitation (mm d^{-1}; 1990–2020) in the ERA5 with the CMFD

Table 2 The four cases of precipitation simulation in the HSS

ERA5	Observation	
	Rainy	No rainy
Rainy	f_{RR}	f_{RN}
No rain	f_{NR}	f_{NN}

performs better to forecast the precipitation in the TRHR than the TRMM. The HSS is higher in the YERHR and smaller in the LARHR.

There is uncertainty in the ERA5 dataset in describing the rainy season precipitation over the TRHR, such as ignoring the strong precipitation events and overestimating the total precipitation. It is a common issue in the reanalysis dataset, probably related to the observational uncertainties introduced by data assimilation schemes and the terrain smooth due to the rough resolutions (Trenberth et al. 2011). The ERA5 generally reproduces the temporal-spatial distribution of the rainy season in the TRHR. In this study, it is reasonable using the ERA5 dataset to explore the interannual variations of the precipitation and learn the hydrology process in the TRHR and all three sub-regions, which help us to reach the consensus on the climatic precipitation over the TRHR and its interannual variation mechanisms.

3.2 Spatiotemporal variations of the precipitation

(1) Linear trend of the rainy season precipitation in the TRHR

The climatological mean precipitation in the TRHR during the rainy season is 471.4 mm from 1990 to 2020. The value is 561.3 mm in the LARHR, 501.9 mm in the YERHR, and 461.9 mm in the YARHR. The precipitation shows a great increasing trend in the TRHR and the three sub-source regions, with a rate of 17.8 mm decade^{-1}

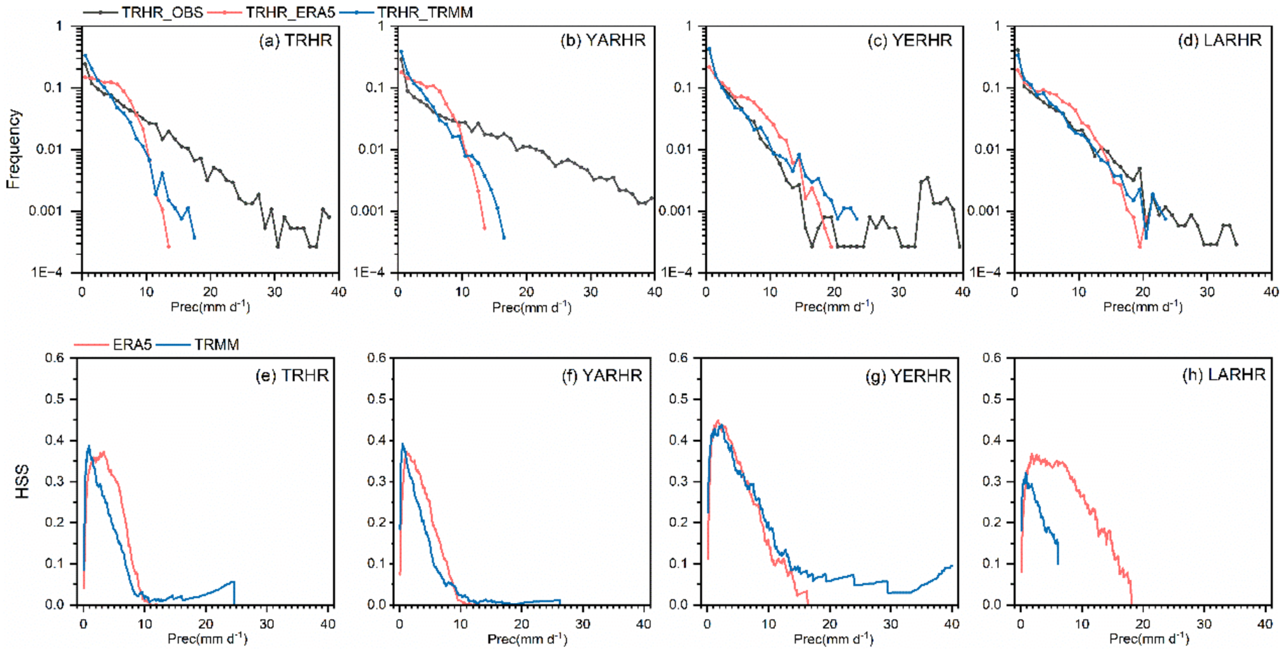

Fig. 3 **a** Precipitation frequency during the rainy season in the ERA5, TRMM and observations; **b** HSS for the daily precipitation in the ERA5 and TRMM over the TRHR and three sub-source regions

(TRHR) , 15.6 mm decade^{-1} (YARHR) , 21.2 mm decade^{-1} (YERHR) , and 18.2 mm decade^{-1} (LARHR) , respectively (Fig. 4).

The time series of precipitation in the TRHR are decomposed by the EEMD into three IMF components and one Residual. The first IMF component which has a high frequency is usually omitted (Basha et al. 2015). The second and third IMF components show periodical oscillations at the periods of 6.2-year and 15.5-year, respectively (Fig. 5b, c). During the recent 31 years, the magnitude of precipitation oscillations gradually decreases at the 6.2-year period and increases at the 15.5-year period (Table 3). The precipitation exhibits a similar trend in the YARHR. In the YERHR, the precipitation oscillation magnitudes show an increasing–decreasing trend in both periods. In the LARHR, the precipitation oscillation is weaker during 2000–2010 than in other years at the period of 6.2-year. The period from the IMF3 is only 10.3-year in the region, and the oscillation magnitude continuously decreases from 1990 to 2020. Residuals show the denoising trend of precipitation during 1990–2020 (Fig. 5d–g). The precipitation in the TRHR and the three sub-source regions gradually increases from 1990 to 2020. The increasing trend in the YARHR is strengthened after 2010. In contrast, the trend is constantly weakened in the YERHR in the research period. In the LARHR, the increasing rate shows a trend of increasing–decreasing-increasing.

(B) Spatial distribution of the precipitation variability during the rainy season from daily to inter-annual timescales in the TRHR

The spatial distribution of the precipitation variability (PV) varies from daily to inter-annual timescales. The daily PV decreases from the southeast to the northwest during 1990–2020. The values are more than 5 mm/day in the eastern YERHR, while less than 2 mm/day in the western YARHR. Spatial distribution of the relative importance of PV at different timescales is shown in Fig. 6. It is expressed as a percentage of the daily PV. The PV is larger at the synoptic scale and smaller at the interannual scale. At the synoptic scale, the highest PV is located in the YERHR due to the interplay of complex atmospheric circulations (East Asian monsoon, South Asia monsoon, Westerlies, etc.) in the rainy season (Sang et al. 2013). The active water-heat exchange contributed by the extensive lakes and wetlands in the YERHR, also stimulates the convection motions and precipitation formation (Sugimoto and Ueno 2010). At the monthly scale, the PV in the south and north edges of the TRHR is higher than that in the middle TRHR, which is related to the variability of water vapor transport. The water vapor carried by the South Asian monsoon increases from mid-June to early July and then decreases (Zhou et al. 2005). During the period of the South Asian monsoon outbreaks, the northern water vapor transport retreats to the northwest

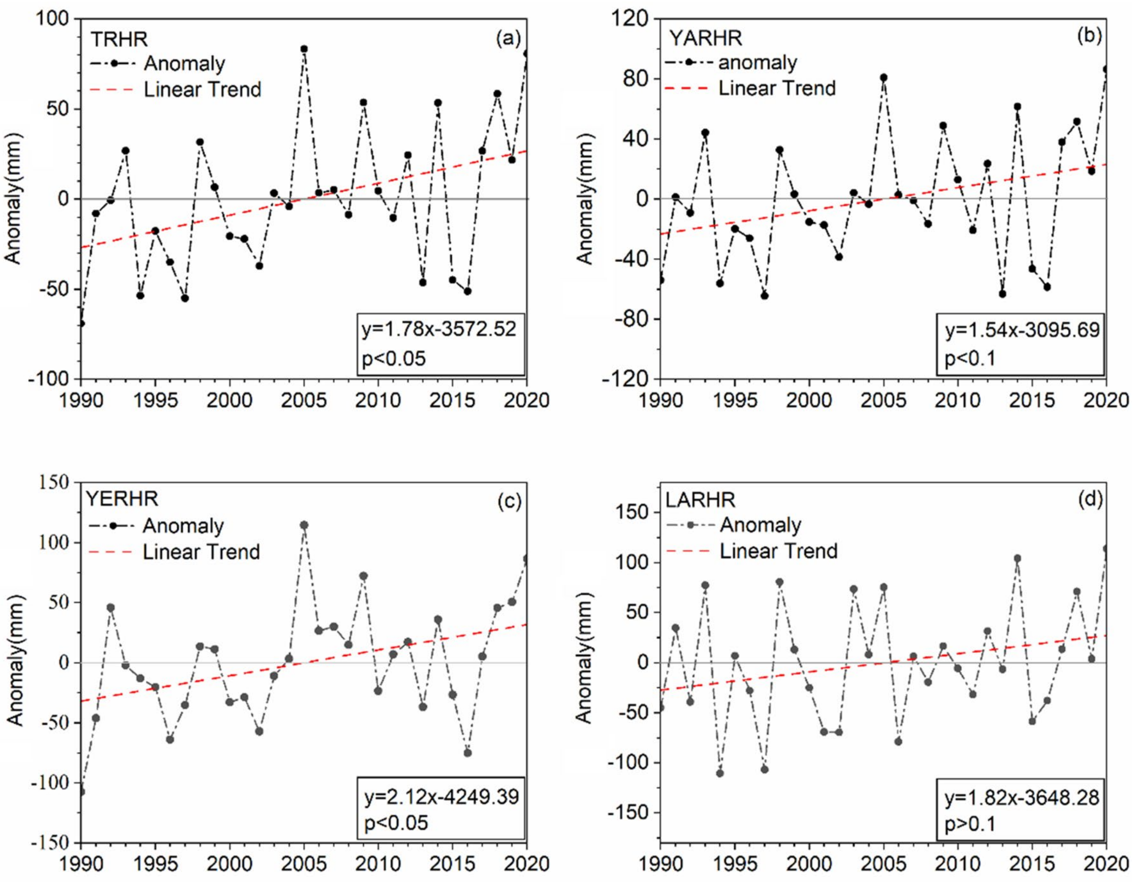

Fig. 4 Linear trends of the rainy season precipitation during 1990–2020 in the TRHR and three sub-source regions (mm yr^{-1})

of the TRHR. The interannual PV decreases from the southwest to the northeast, which is associated with the periodical oscillations of the South Asia monsoon and the westerlies (Wang et al. 2017).

3.3 The moisture flux variations contributing to the TRHR precipitation during the rainy season

The rainy season precipitation in the TRHR is controlled by regional land–atmosphere interactions and external water vapor forcing (Hua et al. 2017). The variations of hydrological components (i.e., precipitation, evaporation and the convergence of the vertically integrated water vapor flux) during the rainy season from 1990 to 2020 are shown in Fig. 7. The rainy season evaporation, which is less than 3 mm d^{-1}, is only approximately 50–60% of the precipitation over all three sub-regions. There is strong convergence of water vapor flux over the TRHR, thus the target region is a moisture sink. To identify the contribution of local evaporation and water vapor transport, the mean Pr during the rainy season is calculated using Eq. 6. We decompose the total precipitation in to Pa and Pe. The schematic diagram of regional water cycle in the TRHR is shown in Fig. 8. The mean Pr in the TRHR is about 6.71%. The F_{in} can restrict nearly 95% of regional precipitation, and the conversion ratio of F_{in} to precipitation is 22.04%. The mean Er in the TRHR is 11.02%. Therefore, approximately 78% of F_{in} and 89% of the local evaporation are transported to the downstream areas. During the past 31 years, with the enhanced water vapor influxes (5.77×10^6 kg s^{-1} decade^{-1}) and the weakened local evaporation (-0.01×10^6 kg s^{-1} decade^{-1}) , the Pr shows a decreasing trend in the TRHR. Meanwhile, the water vapor outflux also increased (4.78×10^6 kg s^{-1} decade^{-1}) , which leads to the wetting trend in the downstream areas.

(1) Contribution of water vapor transport.

Water vapor transport could exchange the water resource between land and sea in high and low latitudes areas, thus playing an important role in precipitation formation (Sun et al. 2020). The rainy season precipitation increase during the recent 31 years is entirely determined by the increase of advected moisture transport. To investigate from which

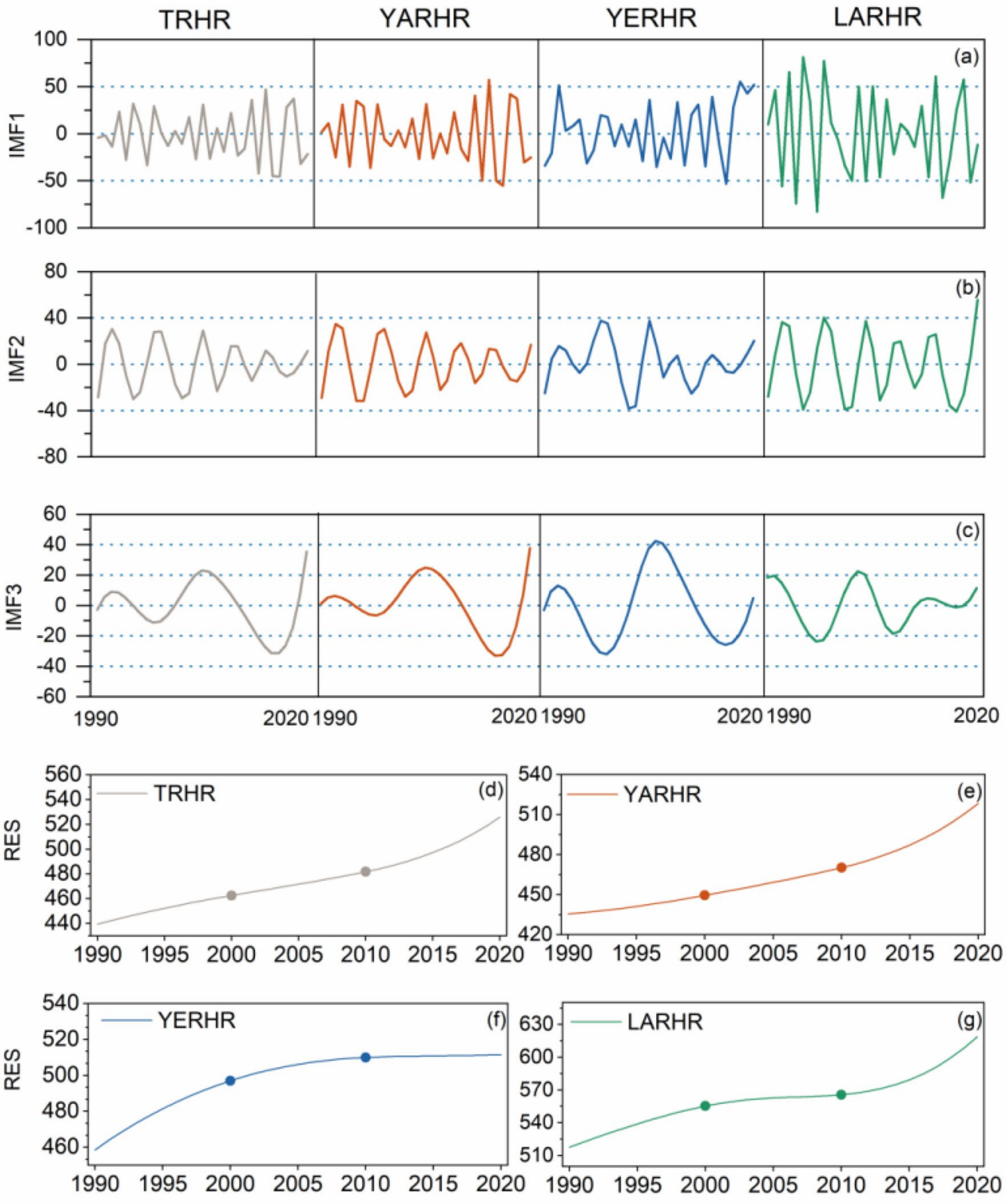

Fig. 5 EEMD of precipitation in the TRHR during 1990–2020. **a**–**c** Are the IMF components, **d**–**g** are residuals

direction the water vapor transported to the TRHR mainly dominates the most to the rainy season precipitation, we divide the water vapor transport by four regional boundaries and calculate these contributions using Eq. 11.

The inter-annual variations of water vapor transport from four boundaries are shown in Fig. 9a. The mean net water vapor influx during the rainy season over the TRHR is 89.82×10^6 kg s^{-1} from 1990 to 2020. The F_S, F_W, F_N and F_E are 66.44×10^6 kg s^{-1}, 67.59×10^6 kg s^{-1}, 28.58×10^6 kg s^{-1} and 72.79×10^6 kg s^{-1}, respectively. Calculating the linear trend of the water vapor transport over the last 31 years, we found that the F_S shows a significant increasing trend, with a rate of 7.61×10^6 kg s^{-1} decade^{-1}. The adverse trend occurs at the F_N with a rate of -5.02×10^6 kg s^{-1} decade^{-1}. The variations of F_W and F_E over the TRHR do not pass the significance test at the 0.05 confidence level.The percentage

Table 3 The oscillation periods, Pearson correlation coefficients, and variance contribution rates of precipitation in the TRHR and three sub-source regions

	Oscillation period (year)			Correlation coefficient			Variance contribution rate (%)		
	IMF1	IMF2	IMF3	IMF1	IMF2	IMF3	IMF1	IMF2	IMF3
TRHR	2.58	6.2	15.5	0.59*	0.47*	0.32	46.3	21.2	17.5
YARHR	2.58	6.2	15.5	0.62*	0.42*	0.30	57.3	22.6	17.9
YERHR	2.81	6.2	15.5	0.74*	0.49*	0.41*	41	15.8	21.4
LARHR	2.81	6.2	10.3	0.75*	0.49*	0.16	66.2	21.9	5.0

*Denotes the correlation coefficient as statistically significant at the 0.05 level

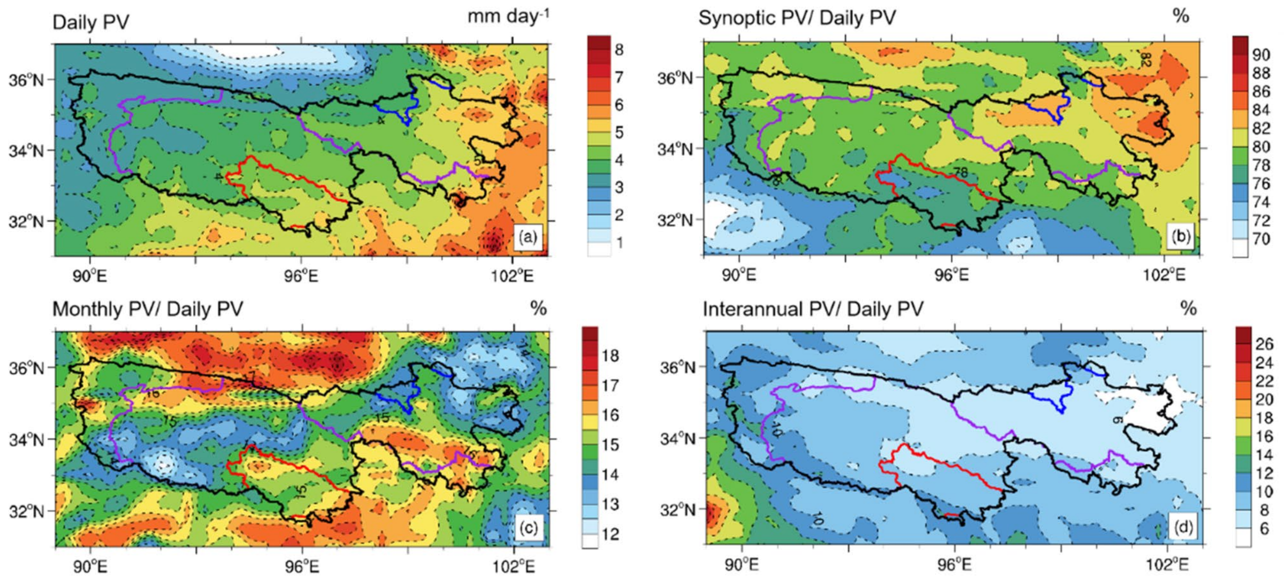

Fig. 6 Daily PV in the rainy season and the relative importance of different time scales over the TRHR. **a** Daily PV during 1990–2020 (mm/day). Synoptic (**b**) , monthly (**c**) , and multi-years (**d**) PV as a percentage of total precipitation variability (%)

contributions of the external water vapor transport at all boundaries and the local evaporation to the precipitation are shown in Fig. 9b. The western and southern influxes, which are carried by the strong westerlies and South Asia monsoon, are major contributors to the mean precipitation during the rainy season over the TRHR. They account for approximately 77% of the rainy season precipitation. The western moisture influx accounts for 60.98%, 64.15% and 70.20% of the precipitation in the YARHR, YERHR and LARHR, respectively (Fig. 9c). The southern and northern moisture influxes contribute 23.45% and 11.53% of the water vapor for the precipitation in the YARHR. The northern water vapor influx contributes approximately 26.47% of the precipitation in the YERHR. The southern water vapor influx accounts for 27.93% of the precipitation in the LARHR. In general, the southwestern water vapor influxes are the most important water vapor source for the precipitation in the TRHR. The contribution of that to the precipitation is the largest in the LARHR, followed by the YARHR, and the least in the YERHR. The precipitation in the YERHR is mainly affected by the northwestern water vapor influxes. By calculating the correlation coefficients between the water vapor influx from the three directions and the precipitation (Table 4) , we found that the northern and southern moisture influxes predominantly regulate the precipitation variations during the 31 years. Larger southern moisture influx and less northern moisture influx promote the precipitation increase in the TRHR during the recent 31 years.

Composite means and linear trends of water vapor transport and specific humidity at 700, 500 and 300 hPa over the TRHR are shown in the left column of Fig. 10. The 700 hPa, 500 hPa, and 300 hPa are chosen as the typical heights for the low, middle, and upper levels in the TRHR, respectively. At 700 hPa, there are three water vapor pathways towards the TRHR: the first is that the warm-humid air from the Indian Ocean and the Bay of Bengal is carried by the South Asian monsoon via the southern and western boundaries into the TRHR. The water vapor conveying is blocked by the Mountain Himalayas, resulting in abundant precipitation on the southern slope of the TP (Fu et al. 2018). The second

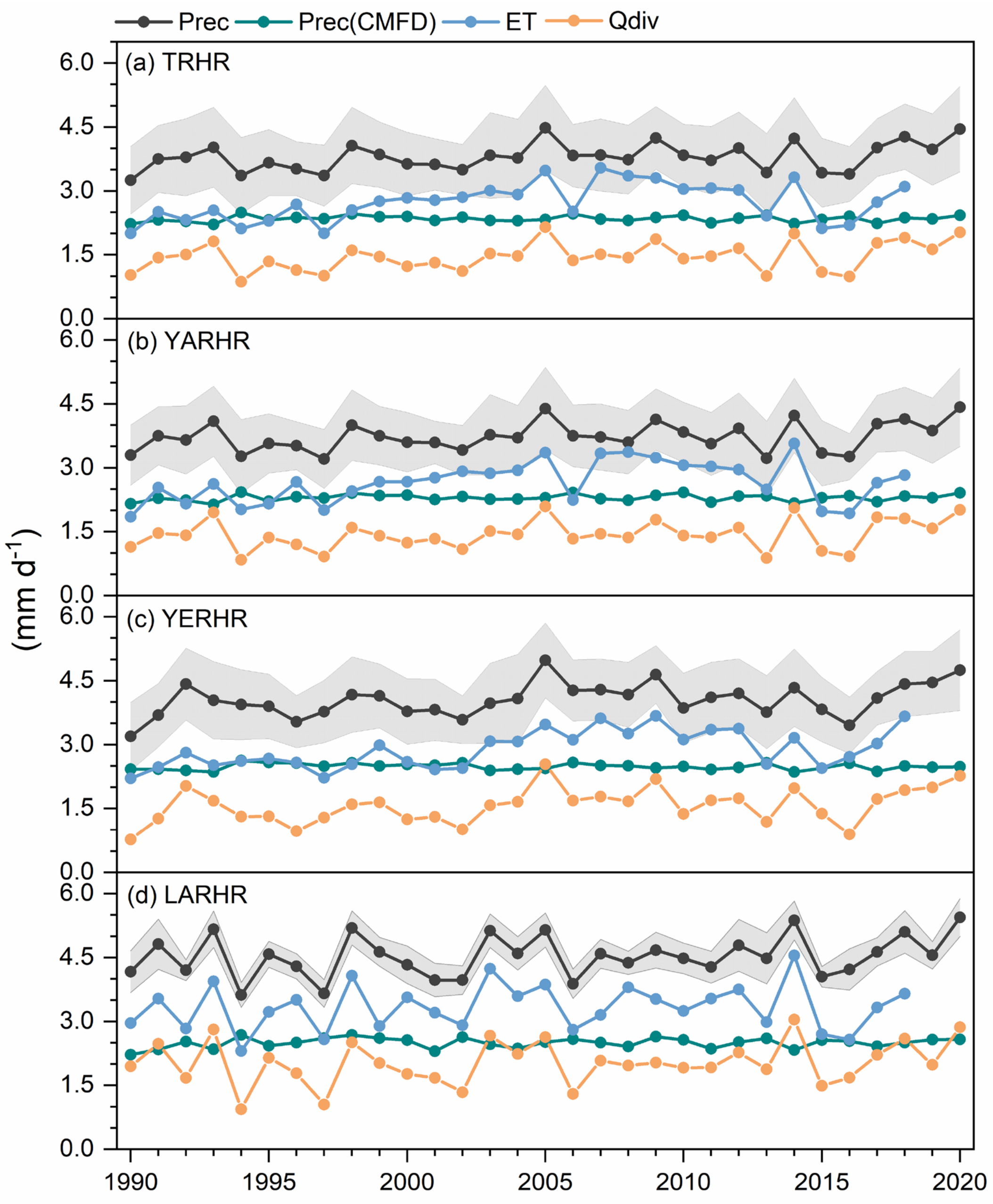

Fig. 7 The rainy season precipitation in the ERA5 (Prec) and the CMFD (Prec (CMFD)) , evaporation (E) , and the convergence of the vertically integrated water vapor fluxes (Qcov) during 1990–2020 over the TRHR and three sub-regions. units: mm d^{-1}. Shaded areas indicate the standard deviation of annual average precipitation in the ERA5

pathway is the southeasterlies transporting the moisture from the south China Sea and the distant tropical oceans via the southern and eastern boundaries. The third pathway is that westerlies transporting the water vapor from the northwestern mid-high latitudes via the northern boundary to the TRHR. At 500 hPa, the water vapor mainly come from the southwest. At 300 hPa, there is a water vapor divergence over the Southern TP. The TRHR is controlled by the westerlies, and the water vapor transports from the west to the east. Overall, the water vapor imports to the TRHR by all four directions at low-level, while the eastern and northern boundaries turn to the water vapor exporting boundaries at the middle and upper levels.

Figure 10 also shows the spatial pattern of the linear regression of the water vapor fluxes during 1990–2020 (the right column). At the low-level, the moisture influxes from all four directions are enhanced. The TRHR shows a more intense wetting trend than other areas on the TP,

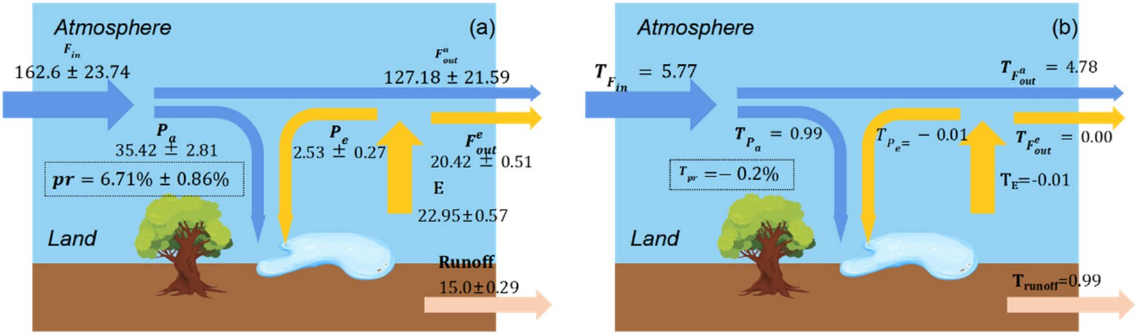

Fig. 8 The schematic diagram of the water cycle (**a**) and its trends (**b**) during the rainy season from 1990 to 2020 over the TRHR (units: **a** 10^6 kg s $^{-1}$; **b** 10^6 kg s $^{-1}$ decade^{-1}). The F_a^{out} is the water vapor outflux from advected water vapor influx; *the*F_e^{out} is the water vapor outflux from local evaporation. The runoff is calculated by the residual of precipitation minus evaporation

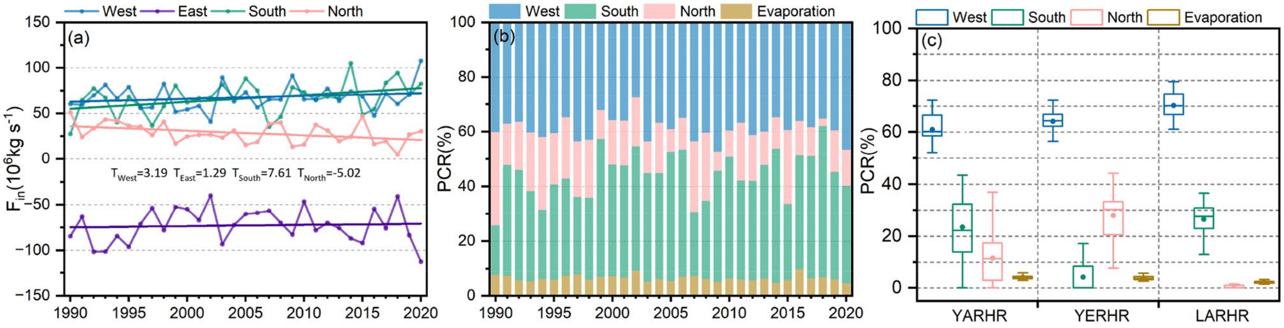

Fig. 9 **a** The linear trends of the water vapor transport from the four boundaries (units: 10^6 kg s^{-1} decade^{-1}) ; **b** The percentage contributions of the local evaporation and the external moisture influxes from four directions to the precipitation during the rainy season from 1990 to 2020 in the TRHR (units: %) ; **c** The percentage contributions in the three sub-source regions (units: %)

Table 4 The contributions of external water vapor transport and evaporation to the mean precipitation (upper half) and the correlation coefficient between the contributions and the precipitation (lower half)

	F_{in}			E
	F_{in}^{w}	F_{in}^{s}	F_{in}^{n}	
PCR_1	0.39	0.37	0.18	0.06
PCR_2	0.39	0.38	0.17	0.06
R (p,F_{in}) $_1$	0.45*	0.77*	−0.37*	−0.30
R (p,F_{in}) $_2$	0.63*	0.69*	−0.31	−0.11

The subscripts 1 and 2 represents the Period 1 (1960–1989) and Period 2 (1990–2020) respectively, which will be mentioned below

*Denotes the correlation coefficient as statistically significant at the 0.05 level

with the rate of more than 0.24 g kg^{-1} decade^{-1}. At the middle-level, the southwestern moisture influxes are also strengthened, while the western influx is weakened. At the upper-level, there is an anomalous water vapor divergence over the eastern TRHR, which could be related to the northward movement of the subtropical westerly jet stream over the North Pacific (Shang et al. 2021; Wang et al. 2017) , resulting in an increase of the eastern and southern water vapor influxes. Moreover, it also represents that the water vapor divergence at the upper level shifted northeastward and more active convection events in the TRHR (Tang et al. 2022). The mean cross-section of meridional moisture conveying during the rainy season from 1990 to 2020 and their linear trends in the TRHR are shown in Fig. 11. In the south of the TRHR, warm–humid air is lifted to the upper level by the large upward motions. Meanwhile, the cold–dry air is sunk by the descent motions in the north of the TRHR. The two airflow converge in the TRHR and stimulates convective events. During 1990–2020, the intensified upward motions in the TRHR carries more water vapor to the upper level, which is conducive to more precipitation formation (Dong et al. 2016).

(2) The contribution of local evaporation.

Evaporation is an important factor that affects the local precipitation, and the effect reflects the intensity of land–atmosphere interactions (Guo et al. 2018; Koster et al. 2004; Seneviratne et al. 2010). The mean evaporation is

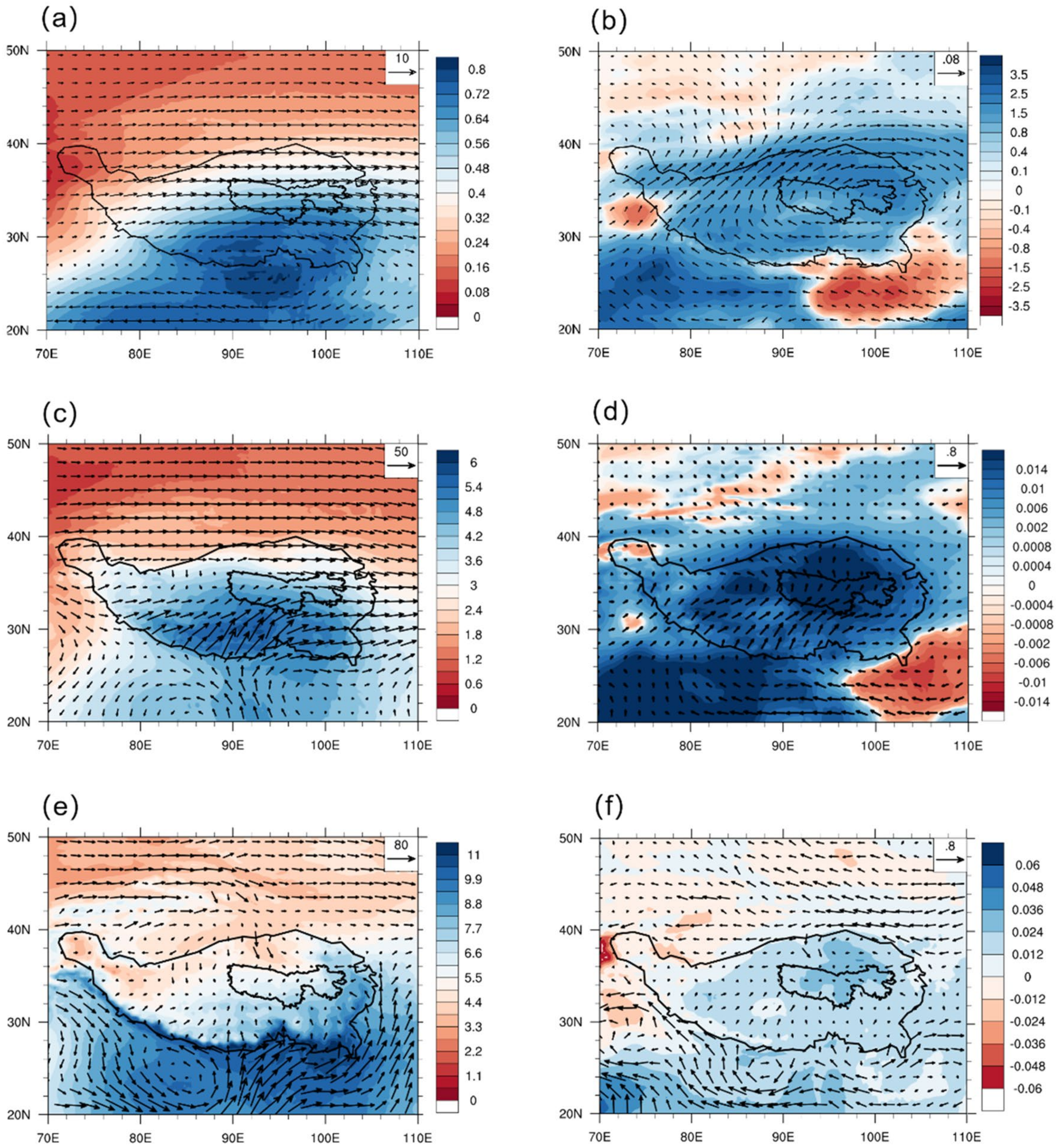

Fig. 10 Climatology and linear trend of water vapor transport (vectors; units: kg m^{-1} s^{-1}, kg m^{-1} s^{-1} yr^{-1}) and specific humidity (contour; units: g kg^{-1}, g kg^{-1} yr^{-1}) at (**a**) , (**b**, $\times 10^{-3}$) 300 hPa, (**c**) , **d** 500 hPa, and **e**, **f** 700 hPa

285 mm in the TRHR during the rainy season from 1990 to 2020, and the spatial distribution is decreasing from the southeast to the northwest (Figure omitted).

The correlations of evaporation and T_{2max} is an adequate diagnosis of the land–atmosphere coupling strength. The rainy season evaporation in the TRHR is positively correlated with T_{2max} (0.50). It demonstrates that the evaporation is more controlled by surface energy budget than soil moisture during the rainy season in the TRHR. The evaporation in the TRHR has significantly positive correlations with the net shortwave radiation (0.53). Previous studies have suggested that the topography could confine the local evaporation and affect the regional water cycling process (Hua et al. 2017; van der Ent et al. 2010). In the western TRHR, with the increasing trend of T_{2max} (0.4 K $decade^{-1}$) , the evaporation increases with the rate of more than 4 mm $decade^{-1}$. The decreasing of net radiation fluxes (-1.3 Wm^{-2} $decade^{-1}$) results in a weakened evaporation in the eastern TRHR.

Although the mean evaporation could explain approximately 6% of the precipitation in the TRHR during the rainy season, the change rate of regional mean evaporation is less

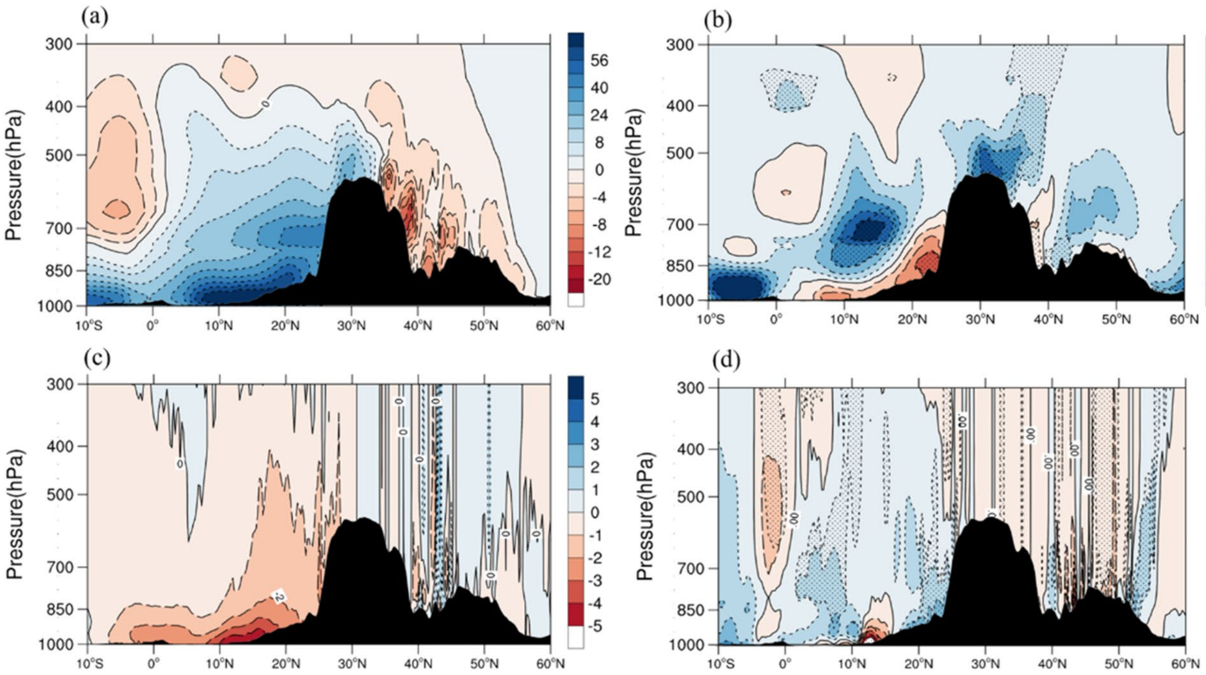

Fig. 11 **a** Pressure–latitude cross-section of the mean meridional water vapor transport (**a** unit: kg m^{-1} s^{-1}) and the vertical velocity (**c** units:10^{-2} m s^{-1} the negative values indicate the upward motions, and the positive values indicate the downward motions) and their linear trends (**b** units: kg m^{-1} s^{-1} yr^{-1}; d units: 10^{-2} m s^{-1} yr^{-1}) during the rainy season from 1990 to 2020. Dots in (**b**) and (**d**) show the regions for which the linear trends are statistically significant at the 0.05 level. The black shaded area shows the cross-section of the terrain, including the TRHR at the latitude of 30–37 °N

than 10% of that in precipitation. The evaporation has little contribution to regulate the precipitation variations at the interannual timescale.

4 Discussion

4.1 Anomalies of the precipitation over the TRHR during the rainy season in wet and dry years

Defining the years in which the rainy season precipitation is one standard deviation higher (lower) than the climatological mean values as anomalous wet (dry) years, we select 2005, 2009, 2014, 2018, and 2020 as anomalous wet years, and 1990, 1994, 1997, 2013, 2015, 2016 as anomalous dry years. The water cycling process during the wet and dry years are shown in Fig. 12b. During the wet years, there are more water vapor influx to the TRHR, especially through the southern boundary (Fig. 12a). The P_a and F_{out} are both increased, while the P_e is decreased. Therefore, the Pr is reduced. The opposite change occurs during the dry years.

The atmospheric circulations over the TRHR determine the water vapor transport (Fig. 13). During the wet year, the two anomalous anticyclones and one anomalous cyclone, which are located over the eastern TRHR, the Indian peninsula, and the Lake Balkhash, respectively, enhancing the western and southern water vapor influxes to the TRHR and leading to the precipitation increase. Meanwhile, the increasing precipitation strengthens the diabatic heating over the TRHR, which in turn affects the formation of the anomalous anticyclones (Jiang et al. 2017; Zhao et al. 2021). In other words, there is a positive feedback process between the precipitation and external water vapor transport. During dry years, the TRHR is affected by the zonal dipole distribution concerning an anomalous anticyclone over Lake Balkhash and an anomalous cyclone over Lake Baikal. The southwestern water vapor influxes are weakened, while the northwestern influxes are strengthened.

4.2 Long-term variations of the rainy season precipitation in the TRHR

We divide the long period of 1960–2020 into two subperiods from 1990. The Period1 (1960–1989) is regarded as a benchmark period that is less affected by the human activities, and the atmospheric water vapor content is relatively stable (Shi et al. 2016; Yi et al. 2013). The Period 2 (1990–2020) is regarded as the research period, which experiences a significant climate change. Precipitation in the TRHR have been found experiencing a dry-to-wet shift

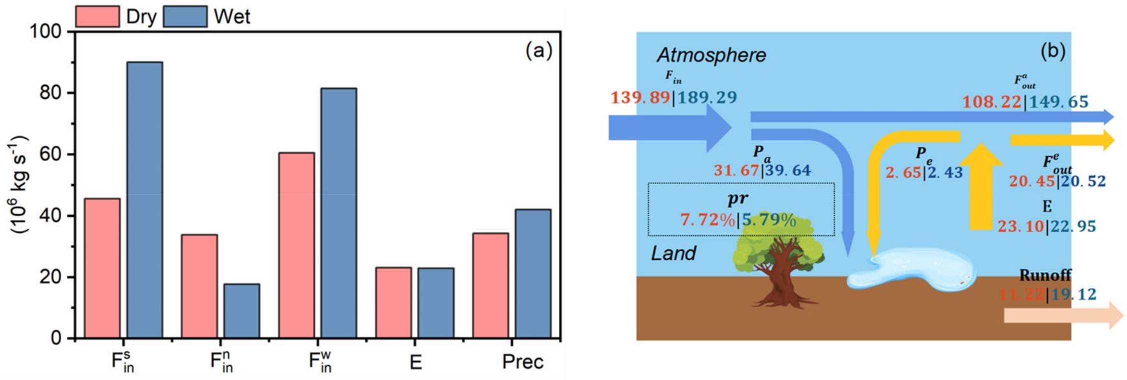

Fig. 12 **a** The mean values of southern, northern, western water vapor influxes, evaporation and precipitation; **b** The schematic diagram of the water cycle during the rainy season in dry (red) and wet (blue) years (units:10^6 kg s^{-1})

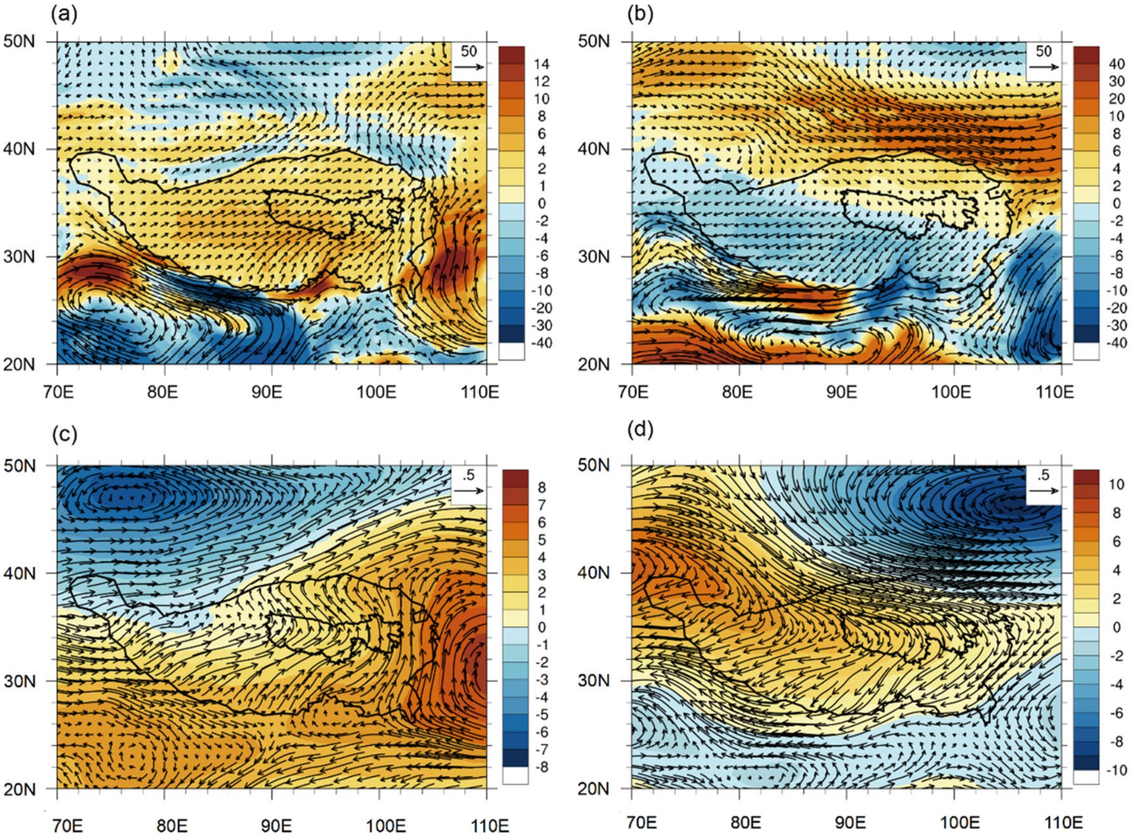

Fig. 13 Anomalies of water vapor transport (units: kg m^{-1} s^{-1}) , 500 hPa wind (vectors, units:m^{-1} s^{-1}) , and geopotential height (contour, units: m, **c**–**d**) in wet (**a**, **c**) and dry (**b**, **d**) years

in around the late 1980s (Liu et al. 2019; Shang et al. 2021). We compare the difference of precipitation controlling factors during the rainy season between the two periods to reveal the main factors for the precipitation variations at the climatology scale.

During the benchmark period, the mean precipitation, evaporation and water vapor influx are 36.53, 22.51 and 164.33 × 10^6 kg s^{-1}, respectively (Table 5). The precipitation and evaporation decrease with the rate of 0.27 × 10^6 kg s^{-1} decade^{-1} and 0.39 × 10^6 kg s^{-1} decade^{-1}, respectively. The moisture influx increases with the rate of 3.02 × 10^6 kg s^{-1} decade^{-1}. Compared with the benchmark period, the mean precipitation increases by 3.9% during the research period, which is contributed by the local evaporation increase

(1.95%) and the advance of the conversion ratio of F_{in} to precipitation (1.15%). During the research period, larger T_{max}, more net radiation fluxes and less cloud cover are the main factors for the evaporation increase, which provide more local water vapor to the precipitation formation. Moreover, more water vapor influx is converted to the precipitation during this period. It makes the most important contribution to the precipitation increase. The vertical distribution of water vapor budget at each boundary in the TRHR is shown in Fig. 14b. It is demonstrated that the highest net water vapor import occurs at 550 hPa. The southern influx, which is served as the main contribution for the precipitation, reaches a peak value at 500 hPa. The western influx mainly presents over the upper level, and controlled by the strong westerlies. The northern influx changes little throughout the whole layer. The eastern influx occurs below 600 hPa, and gradually turns to a water vapor outflux with the altitude increase. Over all, the increase of southern and eastern influxes at low-levels and the decrease of eastern outflux at higher-levels play a key role in the precipitation increase during the research period.

The inter-annual variations of rainy season precipitation in the TRHR are quite different during the two sub-periods. The southern and western water vapor influxes have strong correlations with the precipitation both in the two periods (Table 4). Although the southern and western water vapor influxes increase significantly during the benchmark period, the precipitation decreases with the increase of water vapor outflux. Due to the decrease trend of T_{max} (-0.03 K decade^{-1}) at the benchmark period, combined with the weakened net radiation fluxes (-0.78 W m^{-2} decade^{-1}), the evaporation and the P_e are reduced. During the research period, the increase trend of southern and western water vapor influxes contribute to the precipitation increases.The evaporation theoretically increases with the warming trend (0.42 K decade^{-1}) and the higher wind speed (0.02 m s^{-1} decade^{-1}), while the weakened surface energy budget (-0.72 W m^{-2} decade^{-1}) offset these effect. Nevertheless, the decreasing trend of evaporation and P_e have weakened greatly compared to the benchmark period. Overall, the downward trend of precipitation during the benchmark period is related to the weakened evaporation and net water vapor influx, while the upward trend during the research period is largely dependent on the increase of southern and western moisture influxes.

5 Conclusion

Based on the ERA5 dataset, we estimate the mean precipitation and the inter-annual variations during the rainy season from 1990 to 2020 over the TRHR and three sub-regions. We also identify the contributions of local evaporation and external water vapor transport. Major findings are summarized below.

The rainy season precipitation shows a significant increasing trend with a rate of 17.8 mm decade^{-1} in the TRHR. The increasing rates of precipitation are 15.6 mm decade^{-1}, 21.2 mm decade^{-1} and 18.2 mm decade^{-1} in the YARHR, YERHR, and LARHR, respectively. The trend in the YARHR and LARHR is gradually strengthened during the 31 years, while it is weakened in the YERHR. Moreover, the precipitation in the TRHR experiences periodical oscillations at the quasi-periods of 6.2-year and 15.5-year. The PV in the TRHR shows different spatial patterns from daily to

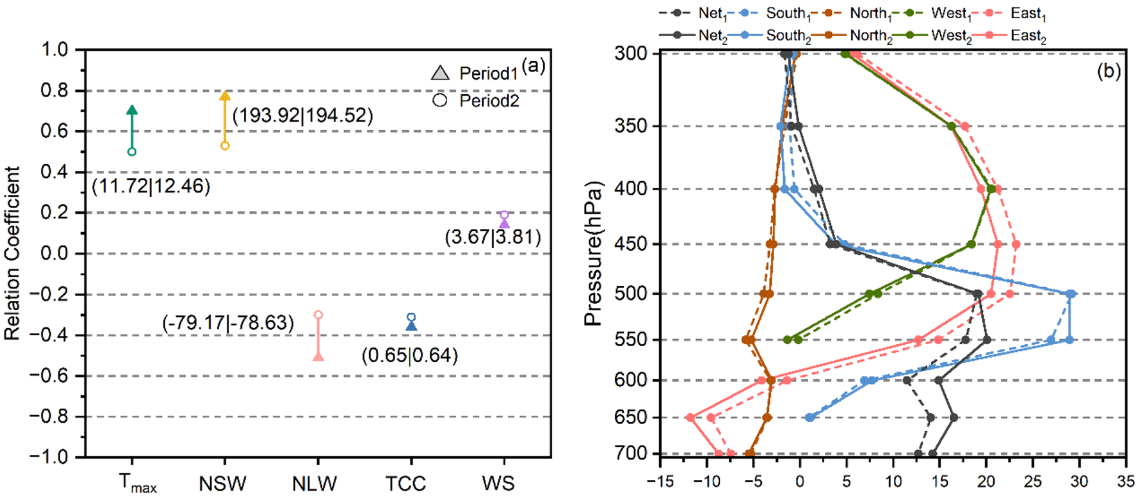

Fig. 14 **a** The correlative coefficient between the evaporation with the T_{max}, net shortwave radiation fluxes (NSW), net longwave radiation fluxes (NLW), total cloud cover (TCC) and wind speed (WS) during the rainy season at the two sub-periods. **b** Vertical distribution of the water vapor budget at each boundary and the net budget (10^6 kg s^{-1}) over the TRHR during the rainy season at the two sub-periods

Table 5 The statistical values of the rainy season precipitation and its associated variables during the two periods in the TRHR

	Statistics	P	E	F_{in}			F_{out}		Runoff
				F_{in}^{w}	F_{in}^{s}	F_{in}^{n}	F_{out}^{a}	F_{out}^{e}	
Period1	μ	36.53	22.51	68.29	66.38	29.66	130.17	20.15	14.02
	σ	2.89	0.85	9.53	18.93	14.26	16.10	0.70	3.24
	T	−0.27	−0.39	1.78	2.38	−1.14	3.20	−0.30	0.12
Period2	μ	37.95	22.95	67.59	66.44	28.58	127.18	20.42	15.00
	σ	2.73	0.56	13.81	17.65	11.03	21.59	0.51	2.85
	T	0.98	−0.01	3.19	7.61	−5.02	4.78	0.002	0.99

The μ, σ, and T represents the mean value (unit:10^6 kg s^{-1}) , standard deviation (unit:10^6 kg s^{-1}) , and linear trend, respectively (unit:10^6 kg s^{-1} $decade^{-1}$)

interannual timescales, and the regional average PV reduces with the timescale increase.

The regional Pr, Fr and Er over the TRHR are calculated using the expanded method of Brubaker et al. (1993) , obtaining the hydrological cycle and its interannual variations. The water vapor transport is the key factor for regulating the rainy season precipitation in the TRHR. The external moisture are mainly transported to the TRHR via the southern, northern and western boundaries. The southern and western moisture influxes can determine 76% of the precipitation in the TRHR. The northern influx controls 18% of the precipitation. The YARHR and LARHR are largely affected by the southwestern influxes, while the YERHR is regulated by the northwestern influxes. The rainy season precipitation is positively correlated with the water vapor influx. The increasing trend of the southwestern influxes from mid-low levels has greatly promoted the precipitation during 1990–2020. Meanwhile, the strengthened ascending motion stimulates more convective events. The local evaporation provides about 6% of the water vapor for the precipitation formation in the TRHR. Owing to the combination of higher temperature, less radiation budget, and larger wind speed, the evaporation changed slightly during the 31 years, and it makes little contribution to the precipitation variations.

The anomalous precipitation in wet and dry years is controlled by the atmospheric circulation. During the dry years, the anomalous cyclone over Lake Barkosh and the anomalous anticyclone over Lake Baikal promotes the F_{in}^{N} and weakens the F_{in}^{S} and F_{in}^{W}, thus the P_a decreases and the P_e increased. The precipitation recycling process is also anomalous active. On the contrary, during the wet years, the F_{in}^{S} is enhanced by the anomalous cyclone over the southwestern and eastern TP, and the P_a increase.

Further,we investigate that the controlling factors for the precipitation at climatology scale. During the benchmark period, the decreasing trend of precipitation is contributed by the downward of the evaporation and net water vapor influx. Compared with the benchmark period, the precipitation increases greatly during the research period, which is affected by the larger Fr and evaporation.

The TRHR is a special region with active land–atmosphere interactions and complex atmospheric circulation, and it is difficult to quantitatively describe the links between the precipitation and other meteorological variables, as well as physical and dynamic processes. In this study, we attempted to break the links into two simple parts based on three assumptions: the first is the relationship between the precipitation and the external moisture transport, which is influenced by the horizontal atmospheric circulation and the vertical motions. The second is the relationship with the local evaporation, involving multiple variables such as temperature, humidity, pressure and wind speed. This decomposition explained the underlying mechanisms affecting regional precipitation variations from the large-scale to local, which could be useful for analyzing the precipitation in complex terrain, and can also be used in climate model simulations to evaluate regional hydrological process. Due to the uncertainty of the ERA5, utilizing the regional climate models with a high spatiotemporal resolution to analyze the land–atmosphere interaction in the TRHR is the focus of the next step.

Author contributions All authors contributed to the study conception and design. Material preparation, data collection and analysis were performed by JZ and QD. The first draft of the manuscript was written by JZ. The manuscript were reviewed and edited by HL and Lujun Xu. All authors read and approved the final manuscript.

Funding This work was supported by the Second Tibetan Plateau Scientific Expedition and Research of China (Grant 2019QZKK0105) and the National Natural Science Foundation of China (Grants 91937301, 41975017 and 41905010).

Data availability The data from the ERA5 reanalysis during this study are openly available from the European Centre for Medium-Range Weather Forecasts at http://cds.climate.copernicus.eu/cdsapp#!/search?type=datasevaporation&text=ERA5. The meteorological station data are openly available from the China Meteorological Administration at http://data.cma.cn/ as cited in Sang et al. (2013). The CMFD precipitation was provided by He et al. (2019) at https://data.tpdc.ac.cn/zh-hans/data/8028b944-daaa-4511-8769-965612652c49/. The TRMM precipitation data are provided from B.Bookhagen at http://www.geog.ucsb.edu/;bodo/TRMM/.

Declarations

Conflict of interest The authors declare that they have no known competing financial interests or personal relationships that could have appeared to influence the work reported in this paper.

References

An WL, Hou SG, Zhang Q, Zhang WB, Wu SY, Xu H, Pang HX, Wang YT, Liu YP (2017) Enhanced recent local moisture recycling on the northwestern Tibetan plateau deduced from ice core deuterium excess records. J Geophys Res-Atmos. https://doi.org/10.1002/2017jd027235

Barros AP, Kim G, Williams E, Nesbitt SW (2004) Probing orographic controls in the Himalayas during the monsoon using satellite imagery. Nat Hazards Earth Syst Sci 4 (1) :29–51. https://doi.org/10.5194/nhess-4-29-2004

Basha G, Ouarda T, Marpu PR (2015) Long-term projections of temperature, precipitation and soil moisture using non-stationary oscillation processes over the UAE region. Int J Climatol 35 (15) :4606–4618. https://doi.org/10.1002/joc.4310

Bisselink B, Dolman AJ (2008) Precipitation recycling: moisture sources over Europe using ERA-40 data. J Hydrometeorol. https://doi.org/10.1175/2008jhm962.1

Bothe O, Fraedrich K, Zhu XH (2010) The large-scale circulations and summer drought and wetness on the Tibetan plateau. Int J Climatol 30 (6) :844–855. https://doi.org/10.1002/joc.1946

Brubaker KL, Entekhabi D, Eagleson PS (1993) Estimation of continental precipitation recycling. J Clim 6 (6) :1077–1089. https://doi.org/10.1175/1520-0442(1993)006%3c1077:Eocpr%3e2.0.Co;2

Cao LG, Pan SM (2014) Changes in precipitation extremes over the "Three-River Headwaters" region, hinterland of the Tibetan Plateau, during 1960–2012. Quat Int 321:105–115. https://doi.org/10.1016/j.quaint.2013.12.041

Chen B, Xu XD, Yang S, Zhang W (2012) On the origin and destination of atmospheric moisture and air mass over the Tibetan Plateau. Theor Appl Climatol 110 (3) :423–435. https://doi.org/10.1007/s00704-012-0641-y

Chen T, Tang GP, Yuan Y, Guo H, Xu ZW, Jiang G, Chen XH (2020) Unraveling the relative impacts of climate change and human activities on grassland productivity in Central Asia over last three decades. Sci Total Environ. https://doi.org/10.1016/j.scitotenv.2020.140649

Cuo L, Li N, Liu Z, Ding J, Liang LQ, Zhang YX, Gong TL (2019) Warming and human activities induced changes in the Yarlung Tsangpo basin of the Tibetan plateau and their influences on streamflow. J Hydrol-Reg Stud. https://doi.org/10.1016/j.ejrh.2019.100625

Curio J, Maussion F, Scherer D (2015) A 12-year high-resolution climatology of atmospheric water transport over the Tibetan Plateau. Earth Syst Dyn 6 (1) :109–124. https://doi.org/10.5194/esd-6-109-2015

Ding YH (2018) Sustainable management and action in china under the increasing risks of global climate change. Engineering 4:301–305. https://doi.org/10.1016/j.eng.2017.12.014

Ding ZY, Wang YY, Lu RJ (2018) An analysis of changes in temperature extremes in the Three River Headwaters region of the Tibetan Plateau during 1961–2016. Atmos Res. https://doi.org/10.1016/j.atmosres.2018.04.003

Dominguez F, Kumar P, Liang XZ, Ting MF (2006) Impact of atmospheric moisture storage on precipitation recycling. J Clim. https://doi.org/10.1175/jcli3691.1

Dong WH, Lin YL, Wright JS, Ming Y, Xie YY, Wang B, Luo Y, Huang WY, Huang JB, Wang L, Tian LD, Peng YR, Xu FH (2016) Summer rainfall over the southwestern Tibetan Plateau controlled by deep convection over the Indian subcontinent. Nature. https://doi.org/10.1038/ncomms10925

Fan XH, Wang MB (2011) Change trends of air temperature and precipitation over Shanxi Province. China Theor Appl Climatol 103 (3–4) :519–531. https://doi.org/10.1007/s00704-010-0319-2

Feng L, Zhou TJ (2012) Water vapor transport for summer precipitation over the Tibetan Plateau: multidata set analysis. J Geophys Res-Atmos. https://doi.org/10.1029/2011jd017012

Fu YF, Pan X, Xian T, Liu GS, Zhong L, Liu Q, Li R, Wang Y, Ma M (2018) Precipitation characteristics over the steep slope of the Himalayas in rainy season observed by TRMM PR and VIRS. Clim Dyn 51 (5–6) :1971–1989. https://doi.org/10.1007/s00382-017-3992-3

Gao YH, Cuo L, Zhang YX (2014) Changes in moisture flux over the Tibetan Plateau during 1979–2011 and possible mechanisms. J Clim 27 (5) :1876–1893. https://doi.org/10.1175/jcli-d-13-00321.1

Gao YH, Xiao LH, Chen DL, Xu JW, Zhang HW (2018) Comparison between past and future extreme precipitations simulated by global and regional climate models over the Tibetan Plateau. Int J Climatol 38 (3) :1285–1297. https://doi.org/10.1002/joc.5243

Guillod BP, Orlowsky B, Miralles DG, Teuling AJ, Blanken PD, Buchmann N, Ciais P, Ek M, Findell KL, Gentine P, Lintner BR, Scott RL, Van den Hurk B, Seneviratne SI (2014) Land-surface controls on afternoon precipitation diagnosed from observational data: uncertainties and confounding factors. Atmos Chem Phys 14 (16) :8343–8367. https://doi.org/10.5194/acp-14-8343-2014

Guo L, Klingaman NP, Demory ME, Vidale PL, Turner AG, Stephan CC (2018) The contributions of local and remote atmospheric moisture fluxes to East Asian precipitation and its variability. Clim Dyn 51 (11–12) :4139–4156. https://doi.org/10.1007/s00382-017-4064-4

Harding KJ, Snyder PK (2012) Modeling the atmospheric response to irrigation in the great plains. Part II: The precipitation of irrigated water and changes in precipitation recycling. J Hydrometeorol. https://doi.org/10.1175/jhm-d-11-099.1

He ZH, Yang L, Tian FQ, Ni GH, Hou AZ, Lu H (2017) Intercomparisons of rainfall estimates from TRMM and GPM multisatellite products over the upper mekong river basin. J Hydrometeorol 18 (2) :413–430. https://doi.org/10.1175/jhm-d-16-0198.1

He J, Yang K, Tang WJ, Lu H, Qin J, Chen YY, Li X (2020) The first high-resolution meteorological forcing dataset for land process studies over China. Sci Data 7:1. https://doi.org/10.1038/s41597-020-0369-y

Heikkila U, Sandvik A, Sorteberg A (2011) Dynamical downscaling of ERA-40 in complex terrain using the WRF regional climate model. Clim. Dyn 7 (8) :1551–1564. https://doi.org/10.1007/s00382-010-0928-6

Hersbach H, Bell B, Berrisford P, Hirahara S, Horanyi A, Munoz-Sabater J, Nicolas J, Peubey C, Radu R, Schepers D, Simmons A, Soci C, Abdalla S, Abellan X, Balsamo G, Bechtold P, Biavati G, Bidlot J, Bonavita M, De Chiara G, Dahlgren P, Dee D, Diamantakis M, Dragani R, Flemming J, Forbes R, Fuentes M, Geer A, Haimberger L, Healy S, Hogan RJ, Holm E, Janiskova M, Keeley S, Laloyaux P, Lopez P, Lupu C, Radnoti G, de Rosnay P, Rozum I, Vamborg F, Villaume S, Thepaut JN (2020) The ERA5 global reanalysis. Quart Q J R Meteorol Soc 146 (730) :1999–2049. https://doi.org/10.1002/qj.3803

Houze RA, Wilton DC,Smull BF (2007) Monsoon convection in the Himalayan region as seen by the TRMM Precipitation Radar. Q J Roy Meteor Soc 133(627):1389–1411. https://doi.org/10.1002/qj.106

Hua LJ, Zhong LH, Ke ZJ (2017) Characteristics of the precipitation recycling ratio and its relationship with regional precipitation in China. Theor Appl Climatol 127 (3–4) :513–531. https://doi.org/10.1007/s00704-015-1645-1

Huang NE, Shen Z, Long SR, Wu MLC, Shih HH, Zheng QN, Yen NC, Tung CC, Liu HH (1998) The empirical mode decomposition and the Hilbert spectrum for nonlinear and non-stationary time series analysis. P Roy Soc A-Math Phy 454 (1971) :903–995. https://doi.org/10.1098/rspa.1998.0193

Huffman GJ, Adler RF, Bolvin DT, Gu GJ, Nelkin EJ, Bowman KP, Hong Y, Stocker EF, Wolff DB (2007) The TRMM multisatellite precipitation analysis (TMPA) : Quasi-global, multiyear, combined-sensor precipitation estimates at fine scales. J Hydrometeorol 8 (1) :38–55. https://doi.org/10.1175/jhm560.1

Jiang XW, Ting MF (2017) A Dipole Pattern of Summertime Rainfall across the Indian Subcontinent and the Tibetan Plateau. J Clim 30 (23) :9607–9620. https://doi.org/10.1175/jcli-d-16-0914.1

Joswiak DR, Yao TD, Wu GJ, Tian LD, Xu BQ (2013) Ice-core evidence of westerly and monsoon moisture contributions in the central Tibetan Plateau. J Glacior 59 (213) :56–66. https://doi.org/10.3189/2013JoG12J035

Koster RD, Dirmeyer PA, Guo ZC, Bonan G, Chan E, Cox P, Gordon CT, Kanae S, Kowalczyk E, Lawrence D, Liu P, Lu CH, Malyshev S, McAvaney B, Mitchell K, Mocko D, Oki T, Oleson K, Pitman A, Sud YC, Taylor CM, Verseghy D, Vasic R, Xue YK, Yamada T, Team G (2004) Regions of strong coupling between soil moisture and precipitation. Science 305 (5687) :1138–1140. https://doi.org/10.1126/science.1100217

Li SC, Li DL, Zhao P, Zhang GQ (2009) The climatic characteristics of vapor transportation in rainy season of the origin area of three rivers in Qinghai-Xizang Plateau (In Chinese). Acta Mevaporationeorologica Sinica 67:591–598

Li MJ, Zhang XQ, Xie CY (2014) Cause analysis on typical anomalous year of water vapor in the upper troposphere over Qinghai-Xizang Plateau (In Chinese). Plateau Meteorol 33:1197–1203

Liang LQ, Li LJ, Liu CM, Cuo L (2013) Climate change in the Tibetan Plateau three rivers source region: 1960–2009. Int J Climatol. https://doi.org/10.1002/joc.3642

Liu XQ, Wu ZZ, Liu YS, Zhao XZ, Rui Y, Zhang J (2019) Spatial-temporal characteristics of precipitation from 1960 to 2015 in the Three Rivers' Headstream Region, Qinghai, China (In Chinese). Acta Geogr Sin 74:1803–1820

Ma YZ, Lu MQ, Chen HN, Pan MX, Hong Y (2018) Atmospheric moisture transport versus precipitation across the Tibetan Plateau: a mini-review and current challenges. Atmos Res. https://doi.org/10.1016/j.atmosres.2018.03.015

Ma QR, You QL, Ma YJ, Cao Y, Zhang J, Niu MM, Zhang YQ (2021) Changes in cloud amount over the Tibetan Plateau and impacts of large-scale circulation. Atmos Res. https://doi.org/10.1016/j.atmosres.2020.105332

Maussion F, Scherer D, Finkelnburg R, Richters J, Yang W, Yao T (2011) WRF simulation of a precipitation event over the Tibetan Plateau, China—an assessment using remote sensing and ground observations. Hydrol Earth Syst Sci 15 (6) :1795–1817. https://doi.org/10.5194/hess-15-1795-2011

Maussion F, Scherer D, Molg T, Collier E, Curio J, Finkelnburg R (2014) Precipitation seasonality and variability over the Tibetan Plateau as resolved by the high Asia reanalysis. J Clim 27 (5) :1910–1927. https://doi.org/10.1175/jcli-d-13-00282.1

Meng XH, Chen H, Li ZG, Zhao L, Zhou BR, Lv SH, Deng MS, Liu YM, Li GW (2020) Review of climate change and its environmental influence on the three-river regions. Plateau Meteorol 39:1133–1143

Meng XH, Deng MS, Liu YM, Li ZG, Zhao L (2022) Remote sensing-detected changes in precipitation over the source region of three rivers in the recent two decades. Remote Sens. https://doi.org/10.3390/rs14092216

Pendergrass AG, Knutti R, Lehner F, Deser C, Sanderson BM (2017) Precipitation variability increases in a warmer climate. Sci Rep. https://doi.org/10.1038/s41598-017-17966-y

Qie XS, Wu XK, Yuan T, Bian JC, Lu DR (2014) Comprehensive pattern of deep convective systems over the Tibetan Plateau-South Asian Monsoon Region based on TRMM data. J Clim 27 (17) :6612–6626. https://doi.org/10.1175/jcli-d-14-00076.1

Qiu J (2008) The third pole. Nature 454 (7203) :393–396. https://doi.org/10.1038/454393a

Radic V, Hock R, Oerlemans J (2008) Analysis of scaling methods in deriving future volume evolutions of valley glaciers. J Glacior. https://doi.org/10.3189/002214308786570809

Rangwala I, Miller JR (2012) Climate change in mountains: a review of elevation-dependent warming and its possible causes. Clim Change 114 (3–4) :527–547. https://doi.org/10.1007/s10584-012-0419-3

Ren Q, Zhou CY, He JH, Cen SX, Deng MY (2017) Impact of preceding Indian ocean sea surface temperature anomaly on water vapor content over the tibevaporationan plateau moist pool in summer and its possible reason (In Chinese). Chin J Atmos Sci 41:648–658

Roushangar K, Alizadeh F (2018) Entropy-based analysis and regionalization of annual precipitation variation in Iran during 1960–2010 using ensemble empirical mode decomposition. J Hydroinform 20 (2) :468–485. https://doi.org/10.2166/hydro.2018.037

Sang YF, Wang ZG, Liu CM, Gong TL (2013) Temporal-spatial climate variability in the headwater drainage basins of the Yangtze River and Yellow River. China J Clim 26 (14) :5061–5071. https://doi.org/10.1175/jcli-d-12-00523.1

Seneviratne SI, Corti T, Davin EL, Hirschi M, Jaeger EB, Lehner I, Orlowsky B, Teuling AJ (2010) Investigating soil moisture-climate interactions in a changing climate: a review. Earth Sci Rev 99 (3–4) :125–161. https://doi.org/10.1016/j.earscirev.2010.02.004

Shang SS, Zhu GF, Wei JH, Li Y, Zhang K, Li RL, Arnault J, Zhang ZY, Laux P, Yang QY, Dong NP, Gao L, Kunstmann H (2021) Associated atmospheric mechanisms for the increased cold season precipitation over the three-river headwaters region from the late 1980s. J Clim 34 (19) :8033–8046. https://doi.org/10.1175/jcli-d-21-0077.1

Shao QQ, Cao W, Fan JW, Huang L, Xu XL (2017) Effects of an ecological conservation and restoration project in the Three-River Source Region. China J Geogr Sci 27 (2) :183–204. https://doi.org/10.1007/s11442-017-1371-y

Shen SJ, Xiao H, Yang HL, Fu DH, Shu WX (2021) Variations of water vapor transport and water vapor-hydrometeor-precipitation conversions during a heavy rainfall event in the Three-River-Headwater region of the Tibetan Plateau. Atmos Res. https://doi.org/10.1016/j.atmosres.2021.105874

Shi HY, Li TJ, Wei JH, Fu W, Wang GQ (2016) Spatial and temporal characteristics of precipitation over the Three-River Headwaters region during 1961–2014. J Hydrol-Reg Stud 6:52–65. https://doi.org/10.1016/j.ejrh.2016.03.001

Shrivastava R, Dash SK, Hegde MN, Pradeepkumar KS, Sharma DN (2014) Validation of the TRMM Multi Satellite Rainfall Product 3B42 and estimation of scavenging coefficients for I-131 and Cs-137 using TRMM 3B42 rainfall data. J Environ Radioactivity. https://doi.org/10.1016/j.jenvrad.2014.08.011

Simmonds I, Bi DH, Hope P (1999) Atmospheric water vapor flux and its association with rainfall over China in summer. J Clim 12 (5) :1353–1367. https://doi.org/10.1175/1520-0442(1999)012%3c1353:Awvfai%3e2.0.Co;2

Song CY, Wang J, Liu YJ, Zhang L, Ding YH, Li QP, Shen XY, Song YL, Yan YP (2022) Toward role of westerly-monsoon interplay in linking interannual variations of late spring precipitation over the southeastern Tibetan Plateau. Atmos Sci Lett. https://doi.org/10.1002/asl.1074

Su FG, Duan XL, Chen DL, Hao ZC, Cuo L (2013) Evaluation of the global climate models in the CMIP5 over the Tibetan Plateau. J Clim 26 (10) :3187–3208. https://doi.org/10.1175/jcli-d-12-00321.1

Sugimoto S, Ueno K (2010) Formation of mesoscale convective systems over the eastern Tibetan Plateau affected by plateau-scale heating contrasts. J Geophys Res-Atmos. https://doi.org/10.1029/2009jd013609

Sun B, Wang HJ (2014) Moisture sources of semiarid grassland in China using the lagrangian particle model FLEXPART. J Clim 27 (6) :2457–2474. https://doi.org/10.1175/jcli-d-13-00517.1

Sun B, Wang HJ (2018) Interannual variation of the spring and summer precipitation over the three river source region in China and the Associated Regimes. J Clim 31 (18) :7441–7457. https://doi.org/10.1175/jcli-d-17-0680.1

Sun B, Wang HJ (2019) Enhanced connections between summer precipitation over the Three-River-Source region of China and the global climate system. Clim Dyn 52 (5–6) :3471–3488. https://doi.org/10.1007/s00382-018-4326-9

Sun J, Yang K, Guo WD, Wang Y, He J, Lu H (2020) Why has the inner Tibetan Plateau become wetter since the mid-1990s? J Clim 33 (19) :8507–8522. https://doi.org/10.1175/jcli-d-19-0471.1

Tang J, Guo XL, Chang Y, Lu GX, Qi P (2022) Long-term variations of clouds and precipitation on the Tibetan Plateau and its subregions, and the associated mechanisms. Int J Climatol 42 (16) :9003–9022. https://doi.org/10.1002/joc.7792

Taylor CM, de Jeu RAM, Guichard F, Harris PP, Dorigo WA (2012) Afternoon rain more likely over drier soils. Nature. https://doi.org/10.1038/nature11377

Tong K, Su FG, Yang DQ, Zhang LL, Hao ZC (2014a) Tibetan Plateau precipitation as depicted by gauge observations, reanalyses and satellite retrievals. Int J Climatol 34 (2) :265–285. https://doi.org/10.1002/joc.3682

Tong LG, Xu XL, Fu Y, Li S (2014b) Wetland changes and their responses to climate change in the "Three-River Headwaters" Region of China since the 1990s. Energies 7 (4) :2515–2534. https://doi.org/10.3390/en7042515

Trenberth KE (1991) Climate diagnostics from global analyses: conservation of mass in ECMWF analyses. J Clim 4 (7) :707–722. https://doi.org/10.1175/1520-0442(1991)004%3c0707:Cdfgac%3e2.0.Co;2

Trenberth KE, Fasullo JT, Mackaro J (2011) Atmospheric moisture transports from ocean to land and global energy flows in reanalyses. J Clim 4 (18) :4907–4924. https://doi.org/10.1175/2011jcli4171.1

van der Ent RJ, Savenije HHG, Schaefli B, Steele-Dunne SC (2010) Origin and fate of atmospheric moisture over continents. Water Resour Res 46:9525–9525. https://doi.org/10.1029/2010wr009127

Wang J (2007) Analysis of the characteristics of water resources in the Sanjiangyuan of Qinghai Province (in Chinese). J Water Process Eng 18 (1) :91–94

Wang ZQ, Duan AM, Yang S, Ullah K (2017) Atmospheric moisture budget and its regulation on the variability of summer precipitation over the Tibetan Plateau. J Geophys Res-Atmos 122 (2) :614–630. https://doi.org/10.1002/2016jd025515

Wang J, Liu YJ, Ding YH, Wu ZL (2021) Towards influence of Arabian Sea SST anomalies on the withdrawal date of Meiyu over the Yangtze-Huaihe River basin. Atmos Res. https://doi.org/10.1016/j.atmosres.2020.105340

Wei JF, Dirmeyer PA (2019) Sensitivity of land precipitation to surface evapotranspiration: a nonlocal perspective based on water vapor transport. Geophys Res Lett. https://doi.org/10.1029/2019gl085613

Wilks DS (1995) Statistical methods in the atmospheric sciences: an introduction. Academic Press, Oxford, p 467

Wu GX, Mao JY, Duan AM, Zhang Q (2004) Recent progress in the study on the impacts of Tibetan Plateau on Asian summer climate (In Chinese). Acta Meteor Sin 62:528–540

Wu GX, Liu YM, Liu X, Duan AM, Liang XY (2005) How the heating over the Tibetan Plateau affects the Asian climate in summer (In Chinese). Chin J Atmospheric Sci 29:47–56

Wu YH, Guo LN, Zheng HX, Zhang B, Li MR (2019) Hydroclimate assessment of gridded precipitation products for the Tibetan Plateau. Sci Total Environ 660:1555–1564. https://doi.org/10.1016/j.scitotenv.2019.01.119

Xi Y, Miao CY, Wu JW, Duan QY, Lei XH, Li H (2018) Spatiotemporal changes in extreme temperature and precipitation events in the three-rivers headwater region, China. J Geophys Res-Atmos. https://doi.org/10.1029/2017jd028226

Xu WX, Zipser EJ (2011) Diurnal variations of precipitation, deep convection, and lightning over and east of the eastern Tibetan Plateau. J Clim 24 (2) :448–465. https://doi.org/10.1175/2010jcli3719.1

Xu XD, Lu CG, Shi XH, Gao ST (2008) World water tower: An atmospheric perspective. Geophys Res Lett 35:20. https://doi.org/10.1029/2008gl035867

Xu X, Zhao T, Lu C, Guo Y, Chen B, Liu R, Li Y, Shi X (2014) An important mechanism sustaining the atmospheric "water tower" over the Tibetan Plateau. Atmos Chem Phys 14 (20) :11287–11295. https://doi.org/10.5194/acp-14-11287-2014

Yang K, He J, Tang WJ, Qin J, Cheng CCK (2010) On downward shortwave and longwave radiations over high altitude regions: observation and modeling in the Tibetan Plateau. Agric for Meteorol 150 (1) :38–46. https://doi.org/10.1016/j.agrformet.2009.08.004

Yang K, Wu H, Qin J, Lin CG, Tang WJ, Chen YY (2014) Recent climate changes over the Tibetan Plateau and their impacts on energy and water cycle: a review. Glob Planet Change 112:79–91. https://doi.org/10.1016/j.gloplacha.2013.12.001

Yang K, Tang QH, Lu H (2022) Precipitation recycling ratio and water vapor sources on the Tibetan Plateau. Sci China Earth Sci 65 (3) :584–588. https://doi.org/10.1007/s11430-021-9871-5

Yao TD, Thompson L, Yang W, Yu WS, Gao Y, Guo XJ, Yang XX, Duan KQ, Zhao HB, Xu BQ, Pu JC, Lu AX, Xiang Y, Kattel DB, Joswiak D (2012) Different glacier status with atmospheric circulations in Tibetan Plateau and surroundings. Nat Clim Change 2 (9) :663–667. https://doi.org/10.1038/nclimate1580

Yi XS, Li GS, Yin YY (2013) Spatio-temporal variation of precipitation in the Three-River Headwater Region from 1961 to 2010. J Geogr Sci 23 (3) :447–464. https://doi.org/10.1007/s11442-013-1021-y

You QL, Kang SC, Aguilar E, Yan YP (2008) Changes in daily climate extremes in the eastern and central Tibetan Plateau during 1961–2005. J Geophys Res-Atmos 113:D7. https://doi.org/10.1029/2007jd009389

Yu JW, Li QQ, Ding YH, Zhang J, Wu QY, Shen XY (2022) Long-term trend of water vapor over the Tibetan Plateau in boreal summer under global warming. Sci China Earth Sci 65(4):662–674. https://doi.org/10.1007/s11430-021-9874-0

Zhang S, Hua D, Meng X, Zhang Y (2011) Climate change and its driving effect on the runoff in the "Three-River Headwaters" region. Acta Geogr Sinica. https://doi.org/10.1007/s11442-011-0893-y

Zhang YY, Zhang SF, Zhai XY, Xia J (2012) Runoff variation and its response to climate change in the Three Rivers source region. J Geogr 22 (5) :781–794. https://doi.org/10.1007/s11442-012-0963-9

Zhang Y, Huang WY, Zhong DY (2019) Major moisture pathways and their importance to rainy season precipitation over the

Sanjiangyuan region of the Tibetan Plateau. J Clim 32 (20) :6837–6857. https://doi.org/10.1175/jcli-d-19-0196.1

Zhang C, Tang QH, Chen DL (2017) Recent Changes in the Moisture Source of Precipitation over the Tibetan Plateau. J Clim 30(5):1807–1819. https://doi.org/10.1175/jcli-d-15-0842.1

Zhang WX, Furtado K, Wu PL, Zhou TJ, Chadwick R, Marzin C, Rostron J, Sexton D (2021) Increasing precipitation variability on daily-to-multiyear time scales in a warmer world. Sci Adv 7:31. https://doi.org/10.1126/sciadv.abf8021

Zhao Y, Zhou TJ (2021) Interannual variability of precipitation recycle ratio over the Tibetan Plateau. J Geophys Res-Atmos 126:2. https://doi.org/10.1029/2020jd033733

Zhou CY, Li YQ, Li W, Chen LX (2005) Climatological Characteristics of Water Vapor Transport over Eastern Part of Qinghai-Xizang Plateau and Its Surroundings. Plateau Meteorol (In Chinese) 24:880–888

Zhou TJ, Gao J, Zhan Y, Zhang LX, Zhang WX (2019a) Water vapor transport processes on Asian water tower (In Chinese). Sci Bull 34:1210–1219

Zhou CY, Zhao P, Chen JM (2019b) The interdecadal change of summer water vapor over the Tibetan Plateau and associated mechanisms. J Clim 32 (13) :4103–4119. https://doi.org/10.1175/JCLI-D-18-0364.1

Zhu GF, Chen SJ (2003) Analysis and comparison of mesoscale convective systems over the Qinghai-Xizang (Tibetan) Plateau. Adv Atmos Sci 20(3):311–322

Zhao RY, Chen B, Xu XD (2021) Intensified Moisture Sources of Heavy Precipitation Events Contributed to Interannual Trend in Precipitation Over the Three-Rivers-Headwater Region in China. Front Earth Sci. https://doi.org/10.3389/feart.2021.674037